HHS Public Access

Author manuscript

Cell Rep. Author manuscript; available in PMC 2023 February 20.

Published in final edited form as:

Cell Rep. 2023 January 31; 42(1): 111963. doi:10.1016/j.celrep.2022.111963.

The aryl hydrocarbon receptor cell intrinsically promotes resident memory CD8+ T cell differentiation and function

Joseph W. Dean[1], **Eric Y. Helm**[2], **Zheng Fu**[1], **Lifeng Xiong**[1], **Na Sun**[1], **Kristen N. Oliff**[1], **Marcus Muehlbauer**[3], **Dorina Avram**[4], **Liang Zhou**[1,5,*]

[1]Department of Infectious Diseases and Immunology, College of Veterinary Medicine, University of Florida, Gainesville, FL 32608, USA

[2]Department of Anatomy and Cell Biology, College of Medicine, University of Florida, Gainesville, FL 32608, USA

[3]Division of Gastroenterology, Hepatology and Nutrition, College of Medicine, University of Florida, Gainesville, FL 32608, USA

[4]Department of Immunology, Moffitt Cancer Center, Tampa, FL 33612, USA

[5]Lead contact

SUMMARY

The Aryl hydrocarbon receptor (Ahr) regulates the differentiation and function of $CD4^+$ T cells; however, its cell-intrinsic role in $CD8^+$ T cells remains elusive. Herein we show that Ahr acts as a promoter of resident memory $CD8^+$ T cell (T_{RM}) differentiation and function. Genetic ablation of Ahr in mouse $CD8^+$ T cells leads to increased $CD127^-KLRG1^+$ short-lived effector cells and $CD44^+CD62L^+$ T central memory cells but reduced granzyme-B-producing $CD69^+CD103^+$ T_{RM} cells. Genome-wide analyses reveal that Ahr suppresses the circulating while promoting the resident memory core gene program. A tumor resident polyfunctional $CD8^+$ T cell population, revealed by single-cell RNA-seq, is diminished upon Ahr deletion, compromising anti-tumor immunity. Human intestinal intraepithelial $CD8^+$ T cells also highly express AHR that regulates *in vitro* T_{RM} differentiation and granzyme B production. Collectively, these data suggest that Ahr is an important cell-intrinsic factor for $CD8^+$ T cell immunity.

In brief

*Correspondence: liangzhou497@ufl.edu.

AUTHOR CONTRIBUTIONS

J.W.D. designed the study and analyzed the data. J.W.D., E.Y.H., Z.F., L.X., K.O., and N.S. performed the experiments. M.M. provided human intestinal samples and suggestions. D.A. provided expertise on mouse disease models. J.W.D. and L.Z. wrote the paper with input from all authors. L.Z. conceived and supervised the study.

DECLARATION OF INTERESTS

The authors declare they have no competing interests.

SUPPLEMENTAL INFORMATION

Supplemental information can be found online at https://doi.org/10.1016/j.celrep.2022.111963.

Dean et al. show that Ahr, an environmental sensor, is important for the development and function of a specific immune cell type called tissue resident memory CD8$^+$ T cells. These cells are critical in the response to local infections and tumors.

Graphical Abstract

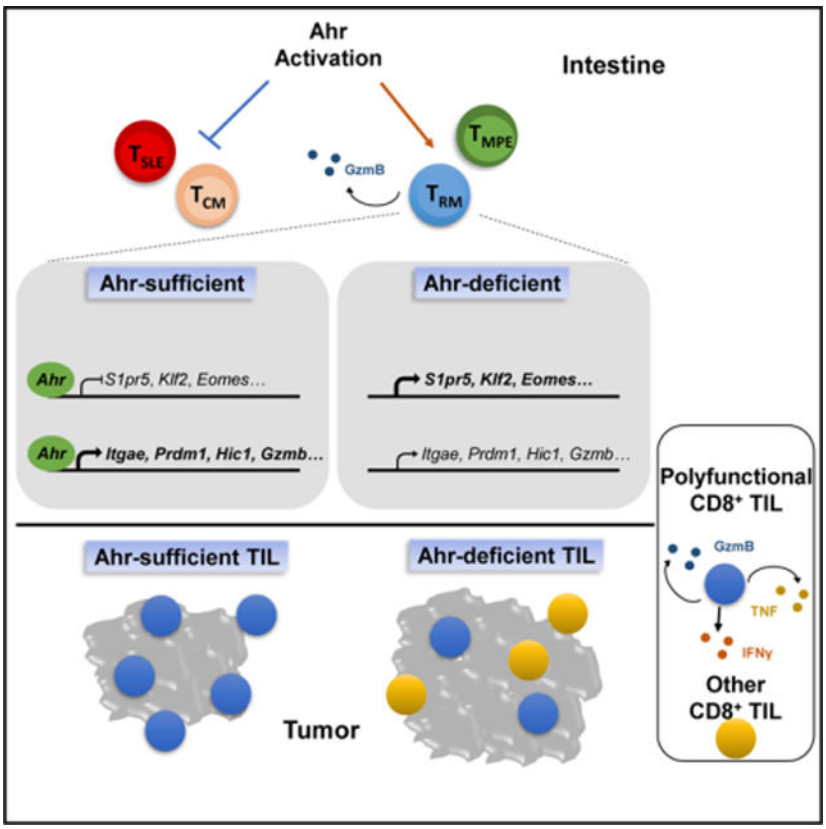

INTRODUCTION

The continuous exposure to various commensals creates a unique “physiological inflammation state” in the gut. Recently, it has been shown that treating “steady-state” specific pathogen-free mice with an antiviral cocktail led to an intestinal intraepithelial (IEL)-specific reduction of most T cell subsets including CD8αβ T cells (hereinafter referred to as CD8$^+$ T cells).[1] These IEL CD8$^+$ T cells are CD69$^+$CD103$^+$ and known as T resident memory (T_{RM}) cells.[2] The lamina propria is home to a diverse population of other CD8$^+$ T cell subsets including CD69$^+$CD103$^+$ CD8$^+$ T cells.[3] Following the recognition of a foreign commensal or pathogen, professional antigen-presenting cells migrate to draining lymph nodes and activate naive CD8$^+$ T cells. Activation of naive CD8$^+$ T cells results in clonal expansion and differentiation into diverse subsets of effector and memory cytotoxic T cell lymphocytes (CTLs).[4,5] This coordinated response helps to eliminate the pathogen and provide long-term protection.

CTLs vary in their phenotype, function, proliferative capacity, longevity, and ability to differentiate into cells conferring long-lived memory.[6] Cells generated during the early phase of expansion likely have a spectrum of phenotypes arising via asymmetric cell division and/or effector cell de-differentiation.[7–10] Killer cell lectin-like receptor subfamily G, member 1 (KLRG1) and IL-7Rα (CD127), have been used as markers to distinguish effector $CD8^+$ T cell subsets based on differences in migration, long-term survival, and memory differentiation potential. $KLRG1^+$ cells, double-positive effector cells ($CD127^+KLRG1^+$, T_{DPE}), and short-lived effector cells ($CD127^-KLRG1^+$, T_{SLE}) cells, while being valuable functional effectors that produce cytolytic molecules such as perforin and granzyme B, at levels similar to other effector subsets,[11] have been described to exhibit limited memory cell differentiation potential.[12–14] In comparison, $KLRG1^-$ cells, double-negative early effector cells ($KLRG1^-CD127^-$, T_{EE}) and memory precursor effector cells ($KLRG1^-CD127^+$, T_{MPE}) cells demonstrate better survival during the contraction phase and maintain stemness, as they are able to differentiate into multiple memory cell lineages.[13–15] This delineation is the canonical model for $CD8^+$ T cell terminal effector vs. memory precursor differentiation; however, recent evidence suggests that there is more nuance and heterogeneity evident at this stage.[16–18]

Memory T cell subsets that survive the contraction phase of infection vary based on their localization and function.[19] T central memory (T_{CM}) cells express the lymph node homing receptors CCR7 and CD62L and have a high proliferative capacity but exhibit low cytotoxicity, while T effector memory (T_{EM}) cells are highly cytotoxic but are less proliferative, do not express CCR7 and CD62L, and therefore survey non-lymphoid tissues in the case of pathogen re-exposure.[20–22] In recent years, T_{RM} cells have gained significant attention because of their ability to remain in the tissue constantly surveilling in case of re-exposure to the same pathogen.[23–25] While the exact ontogeny of T_{RM} cells is not precisely known, the precursor cells poised to differentiate into T_{RM} have been suggested to resemble the classical T_{MPE} phenotype, and CD103 may function as a marker of this precursor population.[3,13,26] However, it has also been shown using a *Klrg1-Cre* fate mapping reporter mouse model that a number of cells that previously expressed KLRG1 and subsequently downregulate it (“ex-KLRG1” cells) give rise to all memory T cell lineages including T_{RM} cells.[16] Runx3, Blimp1, and Hobbit are known transcriptional regulators of the T_{RM} lineage.[27] Runx3 is essential for the differentiation and long-term maintenance of $CD8^+$ T_{RM} cells, while Blimp1 and Hobbit function to suppress Klf2, a transcriptional regulator important for T cell trafficking by promoting expression of S1P1 and CD62L and the T_{CM} cell lineage.[28–30] Upon secondary recognition of cognate antigen, memory cells are able to respond faster than a primary response, and it has recently been show that T_{RM} cells, after re-infection, can leave the tissue and contribute to the systemic immune responses by differentiating into a diverse pool of effector and memory cells.[31,32]

The aryl hydrocarbon receptor (Ahr), a ligand-dependent environmental sensor and transcription factor, can be activated by xenobiotic compounds as well as natural ligands from diet and/or the microbiota.[33,34] Before its role in regulation of the immune system was appreciated, Ahr was shown to mediate the conversion and carcinogenic effects of environmental toxins like 2,3,7,8-tetrachloro-dibenzo-p-dioxin (TCDD). More recently, a physiological role for Ahr has emerged in the regulation of the immune system development

and function via ligands from the microbiome, diet, and host cell metabolism. Compared with well-studied functions in $CD4^+$ and $CD8\alpha\alpha$ T cells,[33,35] the cell-intrinsic role and direct targets of Ahr in $CD8^+$ T cell immune responses remain elusive.

RESULTS

Ahr is expressed by intestinal resident CD8αβ T cells

To more readily detect Ahr expression in different cell populations, we utilized *Ahr*^{dCAIR} mice,[36] in which a GFP reporter was knocked into the endogenous *Ahr* locus under the control of Ahr *cis*-acting regulatory elements. Comparing different tissues, we found that small intestine (SI) intraepithelial lymphocyte (IEL), as well as lamina propria lymphocyte (LPL) fractions in *Ahr*^{dCAIR} mice had the higher levels of GFP expression, indicating *Ahr* transcription, measured by flow cytometry in $CD8^+$ T cells (Figures 1A and 1B). Examination of the different $CD8^+$ T cells displaying markers of effector or memory subsets in the SI LPL (Figure S1A) showed that $CD127^-KLRG1^+$ short-lived effector $CD8^+$ T cells (T_{SLE}) had low *Ahr* expression at a level similar to T_{naive}; however, $CD127^-KLRG1^-$ early effector $CD8^+$ T cells (T_{EE}) and $CD127^+KLRG1^-$ memory precursor effector $CD8^+$ T cells (T_{MPE}) had higher *Ahr* expression (Figure 1C). $CD44^+CD62L^+$ central memory $CD8^+$ T cells (T_{CM}) had a low level of *Ahr* expression, while $CD44^+CD62L^-$ effector $CD8^+$ T cells (T_{EM}) showed higher *Ahr* expression (Figure 1D). Furthermore, $CD69^+CD103^+$ $CD8^+$ T cells (T_{RM}) exhibited the highest level of *Ahr* expression (Figure 1D). Of note, T_{RM} in the SI LPL and IEL had similar levels of *Ahr* expression (Figure S1B). However, in contrast to the LPL (Figure S1A), $CD8^+$ T cells in IEL overwhelmingly consisted of the $CD69^+CD103^+$ T_{RM} population (>90%) (Figure S1G), consistent with higher expression of *Ahr* in IEL than in LPL (Figure 1B). Furthermore, we performed analysis of publicly available RNA-seq data of $CD8^+$ T cell subsets following herpes simplex virus (HSV) infection in various tissues (GSE70813). Consistent with our data, the highest expression level of *Ahr* was detected in T_{RM} ($CD69^+CD103^+$), compared with those in T_{CM} ($CD44^+CD62L^+$), and T_{EM} ($CD44^+CD62L^-$) (Figure S1C). Together, these data suggest in $CD8^+$ T cells Ahr is dynamically expressed along the T_{RM} differentiation pathway in the gut.

Ahr regulates intestinal $CD8^+$ T cell compartment in a cell-intrinsic manner

To further investigate whether Ahr plays a role in the regulation of $CD8^+$ T cell differentiation, we performed a bone marrow chimera experiment. Bone marrow from *Ahr*$^{+/+}$ CD45.1/.2 and *Ahr*$^{-/-}$ CD45.2/.2 donor mice was transferred to half-lethally irradiated CD45.1/.1 mice and allowed to reconstitute for 2 months before flow cytometry analysis of spleen, SI LPL, and IEL (Figure S2A). The percentage of *Ahr*$^{-/-}$-derived cells was reduced in the SI IEL with no difference in the LPL or spleen (Figure S2B). This reduction in total lymphocytes was evidently caused by reduced $CD8^+$ T cells, while $CD4^+$ T cells showed no difference (Figures S2C and S2D), suggesting a role of Ahr in regulating $CD8^+$ T cells in SI IEL. However, there was no difference in the protein level of Ki67 (Figure S2E) or annexin V (Figure S2F) expression in IEL *Ahr*$^{-/-}$ $CD8^+$ T cells examined directly *ex vivo*, suggesting that the observed decrease in these cells might be due to other mechanisms other than compromised cell proliferation or survival.

To further investigate the cell-intrinsic role of Ahr, we developed a genetic model (*Ahr*$^{f/f}$*Cd8*^{cre}) to ablate *Ahr* expression specifically in CD8$^+$ T cells but not in CD4$^+$ T cells by Cre recombinase transgene under the control of the E8I CD8 enhancer region and the *Cd8a* promoter.[37] *Ahr*$^{f/f}$*Cd8*^{cre} mice displayed efficient and specific deletion of *Ahr* in CD8β$^+$ but not in CD8β$^-$ cells (Figures S1D and S1E). Based on examination of different CD8$^+$ T cell subsets in the LPL, we observed T_{SLE} (CD127$^-$KLRG1$^+$) were increased in the *Ahr*$^{f/f}$*Cd8*^{cre} mice (Figure S1F, S2G, and S2H) and T_{RM} (CD69$^+$CD103$^+$) cells were modestly but significantly reduced in the SI IEL (Figures S1G, S2I, and S2J). These data suggest that although Ahr is most likely not a driver that directs the development of T_{RM} cells and/or their maintenance, it plays a cell-intrinsic role in promoting T_{RM} compartment at least at the steady state in the gut.

Ahr suppresses T_{CM} while promoting T_{RM} gene signature in intestinal CD8$^+$ T cells

To determine the role of Ahr in regulation of SI epithelial resident CD8$^+$ T cell compartment, we performed gene profiling analysis of CD8$^+$ T cells from the IEL of *Ahr*$^{f/f}$ and *Ahr*$^{f/f}$*Cd8*^{cre} mice via RNA-seq. Principal component analysis and hierarchical clustering showed distinct separation between different genotypes (Figure S3A). 160 genes were differentially expressed (fragments per kilobase million (FPKM) ≥ 1, fold change ≥ 1.5, q ≤ 0.05) when comparing *Ahr*$^{f/f}$ vs. *Ahr*$^{f/f}$*Cd8*^{cre} mice with roughly equal upregulated (57%) and downregulated (43%) genes, with many being a regulator of or associated with CD8$^+$ T cell memory subset fate (Figure 2A and S3B). Gene set enrichment analysis (GSEA) demonstrated a role for Ahr in promoting the expression of T_{RM}-associated genes while suppressing the expression of T_{CM}-associated genes (Figure 2B).[28] Notably, the magnitude in which the circulating core gene signature was enriched was greater than the enrichment for the resident core gene signature (Figures 2B and 2C). In the absence of Ahr, multiple transcription factors key to the regulation of CD8$^+$ T cell memory development displayed a selectively differential expression pattern. The T_{RM}-promoting factors *Prdm1* and *Hic1*[30,38,39] were downregulated, while the T_{CM}-promoting factors *Eomes* and *Klf2*[40,41] showed a trend of increase with no difference in *Runx3*, *Zfp683* (Hobbit), and *Tbx21* (T-bet) (Figure 2D). Consistently, at the protein level, in the CD69$^+$CD103$^+$ IEL resident CD8$^+$ T cells of *Ahr*$^{f/f}$*Cd8*^{cre} mice, Blimp-1 (encoded by *Prdm1*) was decreased (Figure S3C), while Eomes was increased (Figure S3D) compared with littermate *Ahr*$^{f/f}$ control mice. Together, these transcriptomic changes are consistent with the observed T_{RM} defect and enhancement of T_{CM} cells in the gut of Ahr-deficient mice, suggesting a possibility that Ahr plays a role in CD8$^+$ T cell fate decision.

TGFβ and IL-33 have been previously described to enhance *in vitro* CD69$^+$CD103$^+$ T_{RM}-like cell differentiation.[42,43] Of note, Ahr activation with 6-formylindolo(3.2b) carbazole (FICZ), confirmed by expression of the Ahr direct target gene *Ahrr* (Figure 2I), resulted in a significant enhancement of *in vitro* T_{RM}-like differentiation and reduced differentiation of the CD44$^+$CD62L$^+$ T_{CM}-like cells. These effects were abrogated in *Ahr*$^{-/-}$ and *Ahr*$^{+/+}$ CH223191-treated (Ahr antagonist) CD8$^+$ T cells (Figures 2J, 2K, S4B, and S4C), consistent with a role for Ahr in regulating T_{RM} and T_{CM} differentiation.

Granzymes, especially granzyme B, a well-described effector molecule secreted by cytotoxic lymphocytes to induce apoptosis in target cells,[44] were downregulated at the mRNA level in Ahr-deficient $CD8^+$ cells, while other $CD8^+$ T cell effector molecules including *Tnf*, *Ifng*, *Prf1*, and *Ccl4*, had no change (Figure 2E), suggesting a selective regulation of $CD8^+$ T cell function in the intestine. Consistently, granzyme B, at the protein level on a per cell basis, was also reduced in Ahr-deficient IEL resident $CD8^+$ T cells (Figures 2F and 2G) as well as in the bone marrow chimera model (Figure S4A).

Ahr directly binds DNA to regulate key T_{RM} genes

To elucidate the direct gene targets of Ahr in $CD8^+$ T cells, we performed chromatin immunoprecipitation followed by sequencing (ChIP-seq) of Ahr using *in vitro* T_{RM}-like cells. 10,181 unique Ahr binding locations (peaks) were identified with the majority being located in the intron, intergenic, or promoter regions of genes (Figure 3A). Ahr binding at the promoter was enriched given that the relative abundance of promoter regions in the genome is estimated to be about 1%,[45] and 30% of Ahr peaks were located at the promoter (Figure 3A). Motif enrichment analysis (Figure 3B) showed the canonical Ahr:Arnt binding motif as the top hit. Other transcription factor motifs such as Runx2, ETS, Batf, IRF, and Stat5 were also found to be enriched, suggesting that Ahr might work together with these factors in a complex to bind DNA and regulate target gene transcription. Integration of the ChIP-seq and RNA-seq data by the software package Binding and Expression Target Analysis (BETA)[46] showed that Ahr functioned equally as a transcriptional activator and repressor (Figure 3C). This is different than in other cell types; for example, in ILC2s, Ahr mainly functions as a suppressor,[47] suggesting Ahr acts in a cell type-specific manner to regulate the expression of target genes. BETA direct target prediction identified *Gzmb* together with other T_{RM}-associated genes such as *Itgae*, *Prdm1*, and *Hic1* as top Ahr-activated genes (Figure 3D), while T_{CM}-characteristic genes such as *Klf2*, *Eomes*, *S1pr5*, and *Klrg1* were identified as Ahr-repressed genes (Figure 3D).

To determine whether Ahr DNA binding activity is required for *in vitro* T_{RM}-like differentiation, Ahr-deficient naive $CD8^+$ T cells were transduced with empty vector (MIG-EV), wild-type Ahr (MIG-Ahr), Ahr DNA binding domain single amino acid mutant (MIG-Y9A),[48] or Ahr DNA binding domain deletion mutant (MIG-DbHLH)[49] and then differentiated to T_{RM}-like cells. Compared with MIG-EV control, MIG-Ahr transduction increased $CD69^+CD103^+$ *in vitro* T_{RM}-like differentiation, which was further enhanced by Ahr ligand FICZ treatment (Figure 3E) Both Ahr DNA binding mutants failed to upregulate *Ahrr*, an Ahr direct target gene[50,51] (Figure 3F), and exhibited markedly impaired $CD69^+CD103^+$ $CD8^+$ T cell induction in T_{RM}-like skewing conditions (Figure 3E). These data suggest that Ahr acts in a DNA-binding-dependent manner to promote *in vitro* T_{RM}-like differentiation.

Given that Blimp1 (encoded by *Prdm1*), a well-known factor in promoting tissue residency,[30] was identified as an Ahr direct target (Figure 3D), we further transduced $Ahr^{-/-}$ $CD8^+$ T cells with hCD2-Blimp1. Notably, forced expression of Blimp1 resulted in a marked enhancement of *in vitro* T_{RM}-like differentiation similar to the MIG-Ahr transduced cells (Figures 3G and S5A). These data showed that restoration of Blimp1 levels was

sufficient to rescue the observed *in vitro* T_{RM}-like differentiation defect in Ahr-deficient $CD8^+$ T cells, suggesting that Blimp1 is one of the major downstream targets directly regulated by Ahr during T_{RM} differentiation. It is possible that the *in vitro* over-expression assay would not faithfully recapitulate the *in vivo* microenvironment and thus may not confer the whole T_{RM} gene expression program. Consistent with the regulation of CD69 and CD103 expression by Ahr, we analyzed Ahr ChIP-seq data and showed that Ahr directly bound to both the *Cd69* and *Itgae* (CD103) gene loci (Figures S5B and S5C).

Ahr is a cell-intrinsic promoter of intestinal CD8 T_{RM} during infection

The reduction of $CD69^+CD103^+$ cells in the gut of Ahr-deficient mice under the steady state albeit significant is a modest reduction. Additionally, the results from the *in vitro* T_{RM}-like differentiation could be interpreted as Ahr regulating the expression of CD69 and CD103, not the T_{RM} population as a whole. Indeed, Ahr ChIP-seq analysis showed that Ahr directly bound to both the *Cd69* and *Itgae* (CD103) gene loci (Figures S5B and S5C). Therefore, we sought to determine the role of Ahr in $CD8^+$ T cell responses during infection to further validate these findings. To this end, we utilized a T_{RM}-dependent oral *Listeria monocytogenes*-ovalbumin (*L.m.*-OVA) infection model.[3] The reasons for utilization of this model are 2-fold. It is an intestine-specific infection model that recapitulates human infection, allowing us to corroborate our findings on the role of Ahr in $CD8^+$ T cells under the steady state of the gut; in addition, in combination with OVA-specific transgenic T cells (OTI) it allows for tracking mucosal $CD8^+$ T cell responses in an antigen-specific manner. Host CD45.1/.1 mice were co-transferred with CD45.1/.2 $Ahr^{+/+}$ and CD45.2/.2 $Ahr^{-/-}$ naive OTI $CD8^+$ T cells before infection (Figure 4A). In the SI IEL, CD45.2/.2 $Ahr^{-/-}$ OTI cells were significantly and gradually reduced (Figure 4B). At an effector time point (day 9 post infection), while there was no difference in their frequency in the IEL, $Ahr^{-/-}$ OTI cells already exhibited an imbalanced memory precursor response. Specifically, $CD127^+$ memory precursor populations were reduced in the $Ahr^{-/-}$ OTI cells with a concomitant increase of $CD127^-KLRG1^+$ T_{SLE} (Figure 4C). Immature $CD127^-KLRG1^-$ T_{EE} was also increased in the $Ahr^{-/-}$ OTI cells. The significance of the CD127/KLRG1 memory precursor vs. short-lived effector paradigm in the intestine is not well described. However, during the early stage of infection, $CD69^+CD103^+$ cells could be identified and are suggested to give rise to T_{RM} in the memory phase.[3] Indeed, at this effector time point, $Ahr^{-/-}$ cells had already shown a reduction in the $CD69^+CD103^+$ population with an increase in $CD69^-CD103^-$ cells (Figure 4D), consistent with defective $CD8^+$ T_{RM} differentiation due to Ahr deficiency.

In the spleen, we observed a similar frequency of OTI $CD8^+$ T cells with or without Ahr; however, in MLNs there was an increase in Ahr-deficient OTI $CD8^+$ T cells (Figures S6A and S6B), suggesting the priming of these cells is not impaired. Phenotypic analysis showed that in the absence of Ahr, T_{CM}-like ($CD44^+CD62L^+$) and T_{MPE} ($CD127^+KLRG1^-$) cells were increased in both the spleen and MLNs (Figures S6C–S6J), consistent with the notion that Ahr might function as a T_{CM} suppressor. Of note, in agreement with a previous report,[3] we observed a higher frequency of T_{MPE} in the spleen in oral *L.m.*-OVA infection than those typically observed during systemic infection models. Additionally, while $CD69^+CD103^+$ cells were not present in the mesenteric lymph nodes (MLNs) at this time point, Ahr

deficiency led to a decreased frequency of $CD69^{+}CD103^{-}$ cells that might be poised to become T_{RM}[26] (Figures S6K and S6L), suggesting that Ahr acts early to promote T_{RM}.

To further determine Ahr-mediated regulation of $CD8^{+}$ T cell differentiation in the IEL at the early time point of infection, we performed RNA-seq analysis of $Ahr^{+/+}$ and $Ahr^{-/-}$ OTI $CD8^{+}$ T cells isolated from day 9 post *L.m.*-OVA infected mice. Consistent with our hypothesis that Ahr regulates the differentiation of T_{RM}, we observed, in the absence of Ahr, a suppression of T_{RM} signature gene expression (Figure S7A) with multiple genes overlapping with the steady state RNA-seq analysis (highlighted in red) including the Ahr direct target *Tiparp* and the T_{RM} master regulator *Prdm1* (Figure S7B). Comparison of the two datasets, by principal component analysis, showed that upon addition of the day 9 post-infection data, the steady-state samples were no longer separated based on genotype, but for the infection dataset, $Ahr^{+/+}$ samples were clustered together and distinct from the $Ahr^{-/-}$ samples, suggesting that infection magnifies the gene expression changes between $Ahr^{-/-}$ and $Ahr^{+/+}$ $CD8^{+}$ T cells that were observed under the steady state (Figure S7C). Furthermore, visualization of the transcriptome-wide fold change showed both in number and magnitude greater differential gene expression in the infection dataset compared with steady state (Figure S7D), suggesting that upon challenge with an infectious agent the impact of Ahr deficiency on $CD8^{+}$ transcriptome is greater than that under the steady state. Consistently, the magnitude of the Residency Core Gene Signature enrichment was larger, and the number of differential genes was more compared with the steady state dataset (Figures 2B and 2C vs. S7A and S7B). Collectively, these data suggested that Ahr might play a more prominent role in shaping T_{RM} gene program during infection than it does at steady-state "physiological inflammation" in the gut.

At the memory phase of infection, bona fide T_{RM} is the sole $CD8^{+}$ T cell subset that remains in the IEL by day 34 post infection.[3] Given the reduction of T_{RM} precursor cells observed at day 9, we hypothesized that Ahr-deficient OTI cells would be reduced at this memory time point. Indeed, in the IEL, CD45.2/.2 $Ahr^{-/-}$ OTI cells were significantly reduced at day 34 (Figure 4A). Additionally, CD45.2/.2 $Ahr^{-/-}$ cells produced less granzyme B on a per cell basis compared with CD45.1/.2 $Ahr^{+/+}$ OTI cells (Figures 4E and 4F). Also, at this time point and consistent with the decreased expression of *Prdm1* in Ahr-deficient $CD8^{+}$ T cells analyzed by RNA-seq, IEL OTI cells of $Ahr^{-/-}$ origin exhibited lower levels of Blimp1 staining compared with $Ahr^{+/+}$ cells (Figures S7E and S7F). Collectively these data suggest a critical role of Ahr in promoting T_{RM} cells and their function during infection potentially through regulation of Blimp1 expression.

To determine if the observed reduction of $Ahr^{-/-}$ $CD8^{+}$ T_{RM} cells also was present after a secondary recall challenge, following primary infection, mice were re-infected with *L.m.*-OVA, and then 3 days post re-infection, mice were sacrificed, and analysis of OTI-specific T cell responses was performed (Figure 4A). Consistent with results from the primary infection, in the IEL, CD45.2/.2 $Ahr^{-/-}$ OTI cells were significantly reduced (Figures 4G and 4H) and produced less granzyme B (Figures 4I and 4J). However, in the spleen there was no difference in granzyme B production (Figures S7G and S7H), while $Ahr^{-/-}$ OTI cells from the MLNs showed a trend of decreased granzyme B (Figures S7I and S7J), suggesting that Ahr regulation of $CD8^{+}$ T cell function might be specific to the gut. Together, these

results demonstrate that Ahr is a cell-intrinsic promoter of long-lived, functional T_{RM} cells during intestinal infection.

Single-cell RNA-seq identifies polyfunctional CD8$^+$ T cell population dependent on Ahr

CD8$^+$ tumor-infiltrating lymphocytes (TILs) displaying a T_{RM}-like phenotype have been well described to be critical to the orchestration of potent protective anti-tumor response.[52,53] Therefore, we next investigated the role of Ahr in CD8$^+$ T cells in tumor immunity. Previous literature suggests that Ahr can function as either a tumor promoter or suppressor dependent of the context.[54,55] However, these studies did not address the cell-intrinsic role of Ahr in the tumor, in which perturbation of Ahr in different cell types such as cancer cells or immune cells would inevitably have different outcomes of tumorigenesis. To elucidate the role of Ahr in tumor immunity, B16F10 melanoma cells were injected subcutaneously into *Ahr*$^{-/-}$ mice with *Ahr* germline deletion and into their littermate wild-type *Ahr*$^{+/+}$ mice. CD45$^+$ TILs were purified and subjected to high-throughput single-cell RNA-seq using the 10X Genomics platform. 28 different clusters were identified in both groups with no marked differences between groups. (Figures S8A–S8C).

Given the crucial role of CD8$^+$ T cells in anti-tumor immunity,[28,53] we decided to focus on the impact of Ahr on CD8$^+$ T cells in the tumor microenvironment. Particularly of interest are CD8$^+$ TILs labeled “polyfunctional” that simultaneously produce multiple effector molecules including cytokines, chemokines, and cytotoxic granules. Subsetting on the CD8$^+$ T cell clusters and re-performing dimensionality reduction, clustering, marker gene finding, and visualization resulted in six unique clusters with visual differences between *Ahr*$^{+/+}$ and *Ahr*$^{-/-}$ (Figures 5A and S8D). Ahr-deficient CD8$^+$ T cells were decreased in the polyfunctional and activated (*Ifit1*$^+$ and *Il1b*$^+$) subsets while having an increase in the cluster with a circulating memory-like phenotype (Figure 5A right). Pseudotime analysis by Monocle3 showed that Ahr-deficient CD8$^+$ T cells were less advanced in the pseudotime differentiation trajectory (Figures 5B and 5C), consistent with a role for Ahr in the regulation of CD8$^+$ T cell differentiation. Differential gene expression analysis showed a reduction of genes critical for CD8$^+$ T effector function (i.e., *Gzmb*, *Prf1*, *Ifng*, *Ccl4*, and *Xcl1*), residency-associated membrane receptors (i.e., *Icos* and *Cd69*), and transcriptional modulators (i.e., *Smad7*, *Runx2*, and *Hif1a*) (Figure 5D). Collectively, these results indicate that Ahr is critical to the development of highly activated and polyfunctional CD8$^+$ TILs.

To understand the CD8$^+$ T cell-intrinsic role of Ahr in tumor immunity, *Ahr*$^{f/f}$*Cd8*^{cre} mice were challenged with the aforementioned B16F10 melanoma model and exhibited significantly enhanced tumor growth (Figure 5E) and burden at endpoint (Figure 5F) compared with controls. While there were no differences in their frequency (Figure S8E), CD8$^+$ TILs of *Ahr*$^{f/f}$*Cd8*^{cre} mice were less polyfunctional and produced less granzyme B, IFNγ, and TNF, on a per cell basis. Triple-positive cells (granzyme B$^+$IFNγ^+TNF$^+$) were reduced in the *Ahr*$^{f/f}$*Cd8*^{cre} mice, while triple-negative cells (granzyme B$^-$IFNγ^-TNF$^-$) were increased in the *Ahr*$^{f/f}$*Cd8*^{cre} mice (Figures 5G, 5H, S8E, and S8F). Given the low immunogenicity of the B16F10 model, we sought to validate these findings using the MC38 murine colon carcinoma model. Consistently, *Ahr*$^{f/f}$*Cd8*^{cre} mice exhibited significantly enhanced tumor growth (Figure S9A) and burden at endpoint (Figure S9B) compared with

littermate controls. Furthermore, $CD8^+$ TILs of *Ahr*$^{f/f}$*Cd8*^{cre} mice produced less granzyme B, IFNγ, and TNF on a per cell basis (Figures S9C and S9D) and were less polyfunctional (Figure S9E) in the MC38 tumor model as well. Collectively, these results suggested that Ahr promotes polyfunctional $CD8^+$ TILs in a cell-intrinsic manner.

AHR signaling promotes T_{RM} differentiation and function in human $CD8^+$ T cells

To determine the role of AHR in human $CD8^+$ T cells, we next examined the expression of AHR in human intestine resident $CD8^+$ T cells. Compared with blood circulating $CD45RA^-CD45RO^+$ $CD8^+$ T cells, virtually all IEL resident counterparts were $CD69^+CD103^+$ (Figure 6A). As expected, human IEL resident $CD8^+$ T cells expressed less T-bet,[56] but more AHR (Figures 6B and 6C), consistent with the observation of enrichment of Ahr expression in mouse IEL $CD8^+$ T cells. Next, we performed human *in vitro* T_{RM}-like differentiation using TGFβ and IL-33. Treatment with CH223191, a specific Ahr antagonist,[51] caused a reduction in the frequency of $CD103^+$ cells, whereas FICZ enhanced this population (Figure 6D). Although FICZ or CH223191 treatment did not significantly impact *AHR* expression, TGFβ and IL-33 treatment enhanced *AHR* expression in human $CD8^+$ T cells (Figure 6E). As expected, FICZ treatment increased expression of the AHR target gene *AHR*, while CH223191 suppressed its expression. Notably, FICZ also significantly augmented the expression of the effector gene *GZMB* (Figures 6F and 6G). Together, these results demonstrate an evolutionarily conserved function of AHR in human $CD8^+$ T cells.

DISCUSSION

Proper regulation of $CD8^+$ T cell memory development is critical to long-term protection against morbid infection. Multiple transcription factors have been suggested to contribute to the regulation of this process; however, data describing their cell-intrinsic effects are lacking. A role for Ahr supporting T_{RM} has been previously described.[57] Ahr expression was shown to be higher in skin compared with spleen $CD8^+$ T cells, and Ahr functions to facilitate T_{RM} persistence in the epidermis.[57] Our study provided mechanistic insights into how Ahr regulates the transcriptional programs of $CD8^+$ T cells and elucidated a role for Ahr in early T_{RM} differentiation, specifically in a gut-specific infection model.

Other studies, using an influenza infection model, demonstrated that early-life Ahr activation via TCDD impairs the priming of virus-specific CTLs; however, this phenotype is mediated by regulation of DNA methylation and found to be cell extrinsic.[58,59] Of additional importance, the cellular toxicity and long half-life of TCDD could lead to non-physiological activation of Ahr, thus complicating data interpretation. Given that Ahr is expressed in various cell types and plays a complex role, we ablated Ahr expression specifically in $CD8^+$ T cells. We noted that differences in T_{RM} under the steady state between Ahr-deficient mice and their littermate controls were modest, presumably due to the lack of antigen-specific pathogen exposure and non-competitive environment. Although our data suggest that Ahr plays a cell-intrinsic role in $CD8^+$ T cell differentiation and function, we opted to test this hypothesis in the context of gut infection as well. In the intestine, on day 9 post oral infection, we showed that Ahr-deficient $CD8^+$ T cells exhibited a reduction of T_{RM}

precursors with a concomitant increase in T_{SLE} and T_{CM}-like cells compared with wild-type counterparts. This decrease in precursors led to a marked reduction in the IEL resident T_{RM} cell compartment at the memory time point of day 34 post infection. Of note, for the gut infection model Ahr-deficient OTI $CD8^+$ T cells responded to infection in the presence of an equal number of wild-type OTI $CD8^+$ T cells. This allows for a well-controlled experiment because both are exposed to the same environment and stimuli; however, the magnitude of the observed phenotype could be due to competition. Furthermore, we showed that Ahr functions to promote *in vitro* T_{RM}-like cell differentiation while suppressing the T_{CM} phenotype. Collectively, these data prompted us to conclude that differentiation at least is one of the key mechanisms underlying the defective $CD8^+$ T cell memory development that occurs in the absence of Ahr.

A previous report has shown Ahr is a critical regulator of monocyte differentiation acting to promote dendritic cell differentiation while suppressing macrophage differentiation.[60] In the current study, we demonstrate that in $CD8^+$ T cells, Ahr acts as a cell fate decision regulator to suppress the differentiation of T_{CM} while promoting T_{RM}. Blimp1 is a well-described positive regulator of T_{RM} differentiation and function.[29] We showed that *Prdm1* (Blimp1) is one of the top Ahr-regulated direct target genes in $CD8^+$ T cells, consistent with the role of Ahr in promoting *Prdm1* expression in monocytes.[60] We further showed that forced expression of Blimp1 was able to rescue *in vitro* T_{RM}-like differentiation defect in the absence of Ahr, suggesting that Blimp1 acts downstream of Ahr to regulate $CD8^+$ T cell memory development. It is important to note that $Ahr^{-/-}$ $CD8^+$ T cells were still able to differentiate into $CD69^+CD103^+$ cells *in vitro* and *in vivo*; therefore, Ahr is likely acting as a promoter rather than a main driver of T_{RM} and *in vitro* T_{RM}-like differentiation.

Recent publications describe that Ahr promotes $CD8^+$ T cell exhaustion in tumor immunity.[61,62] However, activated T cells as well as tissue-resident memory cells express many of the exhaustion-associated molecules (PD-1, Tim-3, CTLA-4, etc.).[28,56,63] It is also important to keep in mind that interpretation of the role of Ahr in tumor immunity with ligand treatment has to consider both cell-autonomous and non-autonomous effects, given the cell-specific role of Ahr in different immune cell types that infiltrate the tumor microenvironment, and in the tumor cells as well. It has been reported that when T_{RM} responses are diminished, polyfunctional $CD8^+$ TILs are also reduced,[64,65] consistent with our findings. These polyfunctional tumor-resident memory-like cells have been positively associated with productive anti-tumor immunity.[66–68]

Activation of the Ahr pathway in $CD8^+$ T cells may be of therapeutic interest in the context of infection or cancer immunotherapy when a long-lived tissue-resident memory response is of utmost importance.

Limitations of the study

Our current study represents a serious effort to delineate the cell-intrinsic role of Ahr in $CD8^+$ T cells, specifically in the gut. However, future efforts to understand the role of Ahr in $CD8^+$ T cells in other infection models including skin infection with HSV and systemic lymphocytic choriomeningitis virus (LCMV) infection would help extend our understanding of this biology. Although no difference in the proliferation or cell death was observed in the

intestinal Ahr-deficient T_{RM} cells *ex vivo*, whether Ahr also regulates T_{RM} maintenance in the intestine remains to be carefully determined. Future investigation is needed to elucidate the cell-intrinsic role of Ahr in regulation of T_{RM} maintenance, for example by development of CD8-specific inducible deletion of Ahr mouse model to examine T_{RM} and T_{RM}-like cells in various tissues under the steady state and during infection. Additionally, it is possible that Ahr deficiency could lead to decreased T_{RM} due to aberrant re-entering into circulation after having been in the tissue. In the future, more careful analysis of the recirculation of T_{RM} in the context of Ahr deficiency needs to be done through T_{RM} fate mapping mice as previously described.[32]

STAR★METHODS

RESOURCE AVAILABILITY

Lead contact—Further information and requests for resources and reagents should be directed to and will be fulfilled by the Lead contact, Liang Zhou (liangzhou497@ufl.edu).

Materials availability—This study did not generate new unique reagents.

Data and code availability—All data supporting the findings of this study are available within the article and its supplementary information and from the corresponding author upon reasonable request. The accession number of the RNA-Seq, ChIP-Seq, and scRNA-Seq data reported in this paper have been uploaded to GEO at the accession number: GSE220944. This paper does not report original code. Any additional information required to reanalyze the data reported in this paper is available from the lead contact upon request.

EXPERIMENTAL MODEL AND SUBJECT DETAILS

Human sample collection—Buffy coats from male healthy donors were purchased from Life South Community Blood Centers in accordance with the Institutional Review Boards at the University of Florida (UF IRB #201801563) and PBMCs isolated as described previously.[51] Patients (both male and female) diagnosed with an IBD [Crohn disease (CD) and UC] were recruited for this study. Patients were at least 18 years old and recruited during clinical visits to the Inflammatory Bowel and Celiac Disease Program or before a previously scheduled colonoscopy. Tissue biopsies were taken from the colon. The mucosa was assessed based on frequently used scoring systems (Mayo Score for UC and Simple Endoscopic Score for Crohn Disease for CD). Biopsies collected were labeled as “healthy” based on normal vascularity and lack the presence of edema, erythema, friability, erosions, or ulcerations macroscopically. Intestinal tissue biopsies were collected in complete RPMI and then immediately processed to isolate lamina propria lymphocytes (LPLs) and intraepithelial lymphocytes (IELs) as described previously.[69]

Mice—Mice used in this study were maintained in specific-pathogen-free (SPF) conditions at the University of Florida. All mouse studies were approved by the Institutional Animal Care and Use Committees of the University of Florida. Littermate controls as well as both male and female mice were used for experiments. Mice were used at 8 to 10-week-old age unless otherwise noted. *Ahr*$^{-/-}$,[70] *Ahr*^{dCAIR} 36, *Ahr*$^{f/f}$ 51 were published previously. *EI8Cre*

mice, and OTI TCR transgenic mice were purchased from Jackson Laboratory then crossed with *Ahr*$^{f/f}$ *and Ahr*$^{-/-}$ mice, respectively.

METHOD DETAILS

Lymphocyte isolation and flow cytometry—The isolation of lymphocytes from spleen, peripheral/mesenteric lymph nodes, small and large intestinal lamina propria, and small intestine intraepithelial lymphocytes were performed as previously described.[71] After digestion, cells were further purified from the interphase of 37.5% and 75% Percoll gradient after 20 min spin at 2,500 rpm at room temperature. For flow cytometry analysis, cells were stained using Live and Dead violet viability kit (Invitrogen) or Zombie Aqua fixable viability kit (BioLegend). CD16/32 antibody (Thermo Fisher) was used to block the nonspecific binding followed by surface molecule staining on ice for 30 min. Cells were fixed and permeabilized with Foxp3 staining buffer Kit (eBioscience) for transcription factor staining. For cytokine staining, cells were stimulated with 50 ng/mL PMA and 500 ng/mL ionomycin for 3 h and Brefeldin A (2 μg/mL) was added 2 h before cells were collected. Sample acquisition was performed on BD FACSCantoII or Cytek Aurora flow cytometer and analyzed with FlowJo software (version 10.2).

Adoptive transfers and infection—The spleens of CD45.1/.2 *Ahr*$^{+/+}$ OT-I and CD45.2/.2 *Ahr*$^{-/-}$ OT-I were isolated and single-cell suspensions were generated by mechanical disruption. Naive CD8 (Tcrb^{+}CD8a^{+}CD44^{lo}) OT-I T cells were first enriched using mouse naive CD8^{+} T cell isolation kit (Stemcell Technologies) then further purified using a Sony sorter SH800. Post-sort purity was routinely analyzed and higher than 97%. Purified cells were then mixed in a ratio of 1:1 and 5×10^4 cells were co-transferred 1 day before infection. Mice were infected orally by feeding 2.5×10^9 (primary infection) colony-forming units (CFUs) of *L.m.*-OVA InlAM (kindly provided by B. Sheridan, Stony Brook University) as described previously.[3] At the indicated time points after infection, mice were sacrificed, and tissues were collected for analysis of OT-I T cell responses. For experiments investigating the recall response, following primary infection (>30 day later) mice were re-infected with 2.5×10^{10} CFU of *L.m.*-OVA InlAM. Then, 3 days later mice were sacrificed, and tissues were processed for analysis of OT-I T cell responses.

***In vitro* T_{RM} differentiation—**CD8 T_{RM} cells were differentiated *in vitro* as described previously.[42] Briefly, naive CD8^{+} T cells were purified from splenocytes using mouse naive CD8^{+} T cell isolation kit (Stemcell Technologies) then cultured in RPMI-1640 medium (plus β-mercaptoethanol) supplemented with 10% fetal bovine serum, 1% L-glutamine, 1% penicillin-streptomycin (cRPMI). 100 ng/mL IL-2 and anti-CD3/CD28 coated Dynabeads (Thermo Fisher) at 1:1 cell to bead ratio were added and cells incubated for 48 h. Then media volume was doubled, each well split into a second well, and 5 ng/mL TGF-β and 100 ng/mL IL-33 were added and incubated for another 48 h before harvest for flow cytometry and RT-qPCR analysis.

For human cells, naive CD8^{+} T cells were purified from PBMCs using human naive CD8^{+} T cell isolation kit (Stemcell Technologies) then cultured in cRPMI and treated as above

with the human equivalent Dynabeads and cytokines. FICZ and CH223191 were added at a concentration of 200 nM and 1μM, respectively, as indicated in the text.

Quantitative PCR—Total RNA was isolated with Trizol reagent (Invitrogen). cDNA was synthesized by GoScript™ Reverse Transcription Kit (Promega). Real-time PCR was performed using SYBR Green (Biorad) and different primer sets (Table S1). Reactions were run using the CFX Connect Real-Time PCR Detection System (Biorad). Each specific gene expression was normalized to β-actin expression.

RNA-seq and ChIP-Seq assay and analyses—For RNA-Seq analyses of IEL resident CD8αβ and CD8αα T cells, 2×10^3 sorted CD8αβ and CD8αα T cells from the small intestine IEL of control or *Ahr*$^{f/f}$*Cd8*^{cre} littermate mice were used. RNA was isolated by RNAeasy Micro Kit. cDNA generation was performed with SMART-Seq® HT Kit (Takara). Sequencing libraries were generated with Nextera® XT DNA Library Preparation Kit (Illumina). Libraries were sequenced on an Illumina HiSeq 4000 instrument to produce 50 bp single-end reads. The read mapping and mRNA quantification were performed as previously described.[72] Briefly, FastQC was used to ensure high per-base sequence quality of reads. Sequenced reads were mapped and raw count values quantified with STAR[73] to the *Mus musculus* genome (GRCm38/mm10 assembly). RSEM[74] was used to quantify mRNA expression levels, FPKM aligned reads. Differentially expressed genes (max FPKM ≥1, fold change ≥1.5, q-value ≤0.05) were identified by DESeq2[75] analysis. Gene Set Enrichment Analysis (GSEA)[76,77] were performed using the circulating and resident gene signatures developed previously.[28] Log2 transformed FPKM values were used for principal component analysis in R[78] with the prcomp function and then visualized using the rgl[79] package. Heatmaps were created using the R package pheatmap.[80]

For ChIP-Seq analyses of *in vitro* T_{RM}, cells were differentiated from naive $CD8^+$ T cells as described above. Cells were then treated with FICZ (200 nM) for 4 h before harvest. Afterward, cells were collected and cross-linked with 1% formaldehyde for 15 min. Chromatin was sheared by sonication with Bioruptor Pico (30″ on and 30″ off for 25 cycles) and immunoprecipitated with anti-Ahr antibody (Enzo Life Science) using iDeal ChIP-Seq Kit for transcription factors or True MicroChIP Kit (Diagenode). Eluted DNA was used to generate an indexed library according to the manual of NEBNext Ultra II DNA Library Prep Kit for Illumina (NEB). The library was cleaned up with 1.2x SPRIselect beads (Beckman Coulter) before sequencing on an Illumina HiSeq 4000 instrument to produce 50 bp single-end reads. The read mapping and ChIP-Seq analysis were performed as previously described.[51] Briefly, FastQC was used to ensure high per-base sequence quality of reads. Then ChIP-Seq reads were mapped to the mouse genome (GRCm38/mm10 assembly) with bowtie2 (v2.3.3)[81] and further filtered using samtools (v1.7).[82] The uniquely aligned reads were used to generate bedgraph files (scaled to 10 million reads) using bedtools (v2.25.0)[83] and then were uploaded to UCSC genome browser for visualization. ChIP-Seq peak finding, Motif enrichment analysis, and peak annotation were performed using Homer[84] with default parameters.

Retroviral transduction—Human embryonic kidney (HEK) 293T cells were transfected with retroviral plasmids and the packaging plasmid 10A1 using polyethyleneimine (PEI).

Viral supernatant was collected after transfection. $CD8^+$ T cells were isolated and cultured as described above. After 24 h of culture, retrovirus-containing supernatants supplemented with polybrene (8 μg/mL, Sigma-Aldrich) were added to the cells followed by centrifugation at 2500 rpm for 2 h at 32°C on days 1 and 2. The cells were further cultured under *in vitro* T_{RM}-like differentiation conditions before harvest as indicated in the text.

Plasmids—cDNA of mouse Ahr (1–805 amino acids) was cloned into MIG with hemagglutinin (HA) at the N terminus. For the Ahr Y9A (1–805 amino acids, Y9A), AhrΔbHLH (1–120 amino acids, were deleted) and subcloned into MIG with HA tag. Blimp1-hCD2 plasmid was kindly provided by Dr. Weishan Huang (Louisiana State University).

Tumor model—For the melanoma and MC38 tumor models, mice were injected in the right flank subcutaneously with B16-F10 or MC38 (5×10^5) cells then tumor growth was monitored every other day with a digital caliper. At endpoint, tumors were excised and cut with scissors into <2mm pieces then incubated with collagenase and DNase I for 30 min at 37°C in a shaking incubator. Samples were passed through a 100-μm filter, tumor infiltrating lymphocytes (TILs) were isolated by interphase collection after a 40% and 80% Percoll gradient centrifugation and then analyzed via flow cytometry as described above.

Single cell RNA-Seq analyses—Live $CD45^+$ total TILs were isolated and purified by FACS sorting from a total of 4 mice (2 $Ahr^{+/+}$ and 2 $Ahr^{-/-}$) before being loaded on the chromium controller aiming for a recovery of 10,000 cells. Single Cell 30 reagent kit v3.1 was used for reverse transcription, cDNA amplification, and library construction of gene expression libraries (10x Genomics) according to the manufacturer. For primary scRNA-Seq analysis: alignment, quantification, and quality control were performed using the Cell Ranger Software and default parameters. After quality control and removal of dead cells, doublets, and contaminating melanoma cells (*Pmel* mRNA count >0) a total of 9726 cells remained for downstream analysis. Normalization, cell clustering (resolution = 2), dimensionality reduction, differential expression, visualization, and pseudotime analysis were performed using the R packages Seurat[85] and Monocle.[86] The 3000 most variable features identified with the variance-stabilizing transformation (vst)-method were used for principal component analysis (PCA). Upon inspection of elbowplot and jackstraw plot, the first 20 principal components (PCs) were used for further analysis. Cell type annotation was performed manually by assessment of cluster marker genes.

QUANTIFICATION AND STATISTICAL ANALYSIS

All data are represented as mean ± SEM and have at least n = 3 per group from at least 2 independent experiments (refer to figure legend to detailed information). Unless otherwise noted, statistical analysis was performed with the unpaired Student's t-test or one-way ANOVA with Dunnett's correction for multiple comparisons. For analysis of tumor growth kinetics, linear regression was performed to test if the slopes are significantly different between groups. Statistical analyses were run using GraphPad Prism 8 software package. p values were indicated with asterisks (*p % 0.05; **p % 0.01; ***p % 0.001; ****p % 0.0001).

Supplementary Material

Refer to Web version on PubMed Central for supplementary material.

ACKNOWLEDGMENTS

We thank the entire Zhou and Avram labs for their help and suggestions. We thank John Bostick for analytical assistance as well as Shainal Gandhi and Lauren Dee for their technical assistance. We thank the Flow Cytometry and ICBR core facilities at the University of Florida and the Genomics Facility at the University of Chicago for sequencing service and assistance. Funding: This work was supported by the NIH (R01AI132391 and R01AI157109, L.Z.; R01AI067846 and 5P30CA076292, D.A.; J.W.D was partially supported by T32AI007110). L.Z. was a Pew Scholar in Biomedical Sciences, supported by the Pew Charitable Trusts, and is an Investigator in the Pathogenesis of Infectious Disease, supported by Burroughs Wellcome Fund. This work was made possible, in part, by NIH Instrumentation Grant 1S10 OD021676–01.

REFERENCES

1. Liu L, Gong T, Tao W, Lin B, Li C, Zheng X, Zhu S, Jiang W, and Zhou R (2019). Commensal viruses maintain intestinal intraepithelial lymphocytes via noncanonical RIG-I signaling. Nat. Immunol. 20, 1681–1691. [PubMed: 31636462]
2. Szabo PA, Miron M, and Farber DL (2019). Location, location, location: tissue resident memory T cells in mice and humans. Sci. Immunol 4, eaas9673. [PubMed: 30952804]
3. Sheridan BS, Pham QM, Lee YT, Cauley LS, Puddington L, and Lefranç ois L (2014). Oral infection drives a distinct population of intestinal resident memory CD8(+) T cells with enhanced protective function. Immunity 40, 747–757. [PubMed: 24792910]
4. Williams MA, and Bevan MJ (2007). Effector and memory CTL differentiation. Annu. Rev. Immunol. 25, 171–192. [PubMed: 17129182]
5. Jameson SC, and Masopust D (2018). Understanding subset diversity in T cell memory. Immunity 48, 214–226. [PubMed: 29466754]
6. Kaech SM, and Cui W (2012). Transcriptional control of effector and memory CD8+ T cell differentiation. Nat. Rev. Immunol. 12, 749–761. [PubMed: 23080391]
7. Arsenio J, Metz PJ, and Chang JT (2015). Asymmetric cell division in T lymphocyte fate diversification. Trends Immunol. 36, 670–683. [PubMed: 26474675]
8. Flossdorf M, Rössler J, Buchholz VR, Busch DH, and Höfer T (2015). CD8+ T cell diversification by asymmetric cell division. Nat. Immunol. 16, 891–893. [PubMed: 26287584]
9. Youngblood B, Hale JS, Kissick HT, Ahn E, Xu X, Wieland A, Araki K, West EE, Ghoneim HE, Fan Y, et al. (2017). Effector CD8 T cells dedifferentiate into long-lived memory cells. Nature 552, 404–409. [PubMed: 29236683]
10. Bannard O, Kraman M, and Fearon DT (2009). Secondary replicative function of CD8+ T cells that had developed an effector phenotype. Science 323, 505–509. [PubMed: 19164749]
11. Yuzefpolskiy Y, Baumann FM, Kalia V, and Sarkar S (2015). Early CD8 T-cell memory precursors and terminal effectors exhibit equipotent in vivo degranulation. Cell. Mol. Immunol. 12, 400–408. [PubMed: 25066419]
12. Joshi NS, Cui W, Chandele A, Lee HK, Urso DR, Hagman J, Gapin L, and Kaech SM (2007). Inflammation directs memory precursor and short-lived effector CD8(+) T cell fates via the graded expression of T-bet transcription factor. Immunity 27, 281–295. [PubMed: 17723218]
13. MacKay LK, Rahimpour A, Ma JZ, Collins N, Stock AT, Hafon ML, Vega-Ramos J, Lauzurica P, Mueller SN, Stefanovic T, et al. (2013). The developmental pathway for CD103+ CD8+ tissue-resident memory T cells of skin. Nat. Immunol. 14, 1294–1301. [PubMed: 24162776]
14. Obar JJ, and Lefranç ois L (2010). Early signals during CD8 T cell priming regulate the generation of central memory cells. J. Immunol. 185, 263–272. [PubMed: 20519649]
15. Kaech SM, Tan JT, Wherry EJ, Konieczny BT, Surh CD, and Ahmed R (2003). Selective expression of the interleukin 7 receptor identifies effector CD8 T cells that give rise to long-lived memory cells. Nat. Immunol. 4, 1191–1198. [PubMed: 14625547]

16. Herndler-Brandstetter D, Ishigame H, Shinnakasu R, Plajer V, Stecher C, Zhao J, Lietzenmayer M, Kroehling L, Takumi A, Kometani K, et al. (2018). KLRG1+ effector CD8+ T cells lose KLRG1, differentiate into all memory T cell lineages, and convey enhanced protective immunity. Immunity 48, 716–729.e8. [PubMed: 29625895]

17. Gerlach C, Moseman EA, Loughhead SM, Alvarez D, Zwijnenburg AJ, Waanders L, Garg R, de la Torre JC, and von Andrian UH (2016). The chemokine receptor CX3CR1 defines three antigen-experienced CD8 T cell subsets with distinct roles in immune surveillance and homeostasis. Immunity 45, 1270–1284. [PubMed: 27939671]

18. Milner JJ, Nguyen H, Omilusik K, Reina-Campos M, Tsai M, Toma C, Delpoux A, Boland BS, Hedrick SM, Chang JT, and Goldrath AW (2020). Delineation of a molecularly distinct terminally differentiated memory CD8 T cell population. Proc. Natl. Acad. Sci. USA 117, 25667–25678. [PubMed: 32978300]

19. Mueller SN, Gebhardt T, Carbone FR, and Heath WR (2013). Memory T cell subsets, migration patterns, and tissue residence. Annu. Rev. Immunol. 31, 137–161. [PubMed: 23215646]

20. Sallusto F, Lenig D, Förster R, Lipp M, and Lanzavecchia A (1999). Two subsets of memory T lymphocytes with distinct homing potentials and effector functions. Nature 401, 708–712. [PubMed: 10537110]

21. Sathaliyawala T, Kubota M, Yudanin N, Turner D, Camp P, Thome JJC, Bickham KL, Lerner H, Goldstein M, Sykes M, et al. (2013). Distribution and compartmentalization of human circulating and tissue-resident memory T cell subsets. Immunity 38, 187–197. [PubMed: 23260195]

22. Steinert EM, Schenkel JM, Fraser KA, Beura LK, Manlove LS, Igyártó BZ, Southern PJ, and Masopust D (2015). Quantifying memory CD8 T cells reveals regionalization of immunosurveillance. Cell 161, 737–749. [PubMed: 25957682]

23. Schenkel JM, Fraser KA, Vezys V, and Masopust D (2013). Sensing and alarm function of resident memory $CD8^+$ T cells. Nat. Immunol. 14, 509–513. [PubMed: 23542740]

24. Ariotti S, Hogenbirk MA, Dijkgraaf FE, Visser LL, Hoekstra ME, Song JY, Jacobs H, Haanen JB, and Schumacher TN (2014). T cell memory. Skin-resident memory $CD8^+$ T cells trigger a state of tissue-wide pathogen alert. Science 346, 101–105. [PubMed: 25278612]

25. Schenkel JM, Fraser KA, Beura LK, Pauken KE, Vezys V, and Masopust D (2014). T cell memory. Resident memory CD8 T cells trigger protective innate and adaptive immune responses. Science 346, 98–101. [PubMed: 25170049]

26. Kok L, Masopust D, and Schumacher TN (2021). The precursors of CD8+ tissue resident memory T cells: from lymphoid organs to infected tissues. Nat. Rev. Immunol. 22, 283–293. [PubMed: 34480118]

27. Milner JJ, and Goldrath AW (2018). Transcriptional programming of tissue-resident memory CD8 + T cells. Curr. Opin. Immunol. 51, 162–169. [PubMed: 29621697]

28. Milner JJ, Toma C, Yu B, Zhang K, Omilusik K, Phan AT, Wang D, Getzler AJ, Nguyen T, Crotty S, et al. (2017). Runx3 programs CD8+ T cell residency in non-lymphoid tissues and tumours. Nature 552, 253–257. [PubMed: 29211713]

29. Mackay LK, Minnich M, Kragten NAM, Liao Y, Nota B, Seillet C, Zaid A, Man K, Preston S, Freestone D, et al. (2016). Hobit and Blimp1 instruct a universal transcriptional program of tissue residency in lymphocytes. Science 352, 459–463. [PubMed: 27102484]

30. Rutishauser RL, Martins GA, Kalachikov S, Chandele A, Parish IA, Meffre E, Jacob J, Calame K, and Kaech SM (2009). Transcriptional repressor Blimp-1 promotes CD8+ T cell terminal differentiation and represses the acquisition of central memory T cell properties. Immunity 31, 296–308. [PubMed: 19664941]

31. Fonseca R, Beura LK, Quarnstrom CF, Ghoneim HE, Fan Y, Zebley CC, Scott MC, Fares-Frederickson NJ, Wijeyesinghe S, Thompson EA, et al. (2020). Developmental plasticity allows outside-in immune responses by resident memory T cells. Nat. Immunol. 21, 412–421. [PubMed: 32066954]

32. Behr FM, Parga-Vidal L, Kragten NAM, van Dam TJP, Wesselink TH, Sheridan BS, Arens R, van Lier RAW, Stark R, and van Gisbergen KPJM (2020). Tissue-resident memory CD8+ T cells shape local and systemic secondary T cell responses. Nat. Immunol. 21, 1070–1081. [PubMed: 32661361]

33. Cervantes-Barragan L, Chai JN, Tianero MD, Di Luccia B, Ahern PP, Merriman J, Cortez VS, Caparon MG, Donia MS, Gilfillan S, et al. (2017). Lactobacillus reuteri induces gut intraepithelial CD4+CD8αα+ T cells. Science 357, 806–810. [PubMed: 28775213]
34. Zelante T, Iannitti RG, Cunha C, De Luca A, Giovannini G, Pieraccini G, Zecchi R, D'Angelo C, Massi-Benedetti C, Fallarino F, et al. (2013). Tryptophan catabolites from microbiota engage aryl hydrocarbon receptor and balance mucosal reactivity via interleukin-22. Immunity 39, 372–385. [PubMed: 23973224]
35. Gutiérrez-Vázquez C, and Quintana FJ (2018). Regulation of the immune response by the aryl hydrocarbon receptor. Immunity 48, 19–33. [PubMed: 29343438]
36. Ye J, Qiu J, Bostick JW, Ueda A, Schjerven H, Li S, Jobin C, Chen ZME, and Zhou L (2017). The aryl hydrocarbon receptor preferentially marks and promotes gut regulatory T cells. Cell Rep. 21, 2277–2290. [PubMed: 29166616]
37. Maekawa Y, Minato Y, Ishifune C, Kurihara T, Kitamura A, Kojima H, Yagita H, Sakata-Yanagimoto M, Saito T, Taniuchi I, et al. (2008). Notch2 integrates signaling by the transcription factors RBP-J and CREB1 to promote T cell cytotoxicity. Nat. Immunol. 9, 1140–1147. [PubMed: 18724371]
38. Burrows K, Antignano F, Bramhall M, Chenery A, Scheer S, Korinek V, Underhill TM, and Zaph C (2017). The transcriptional repressor HIC1 regulates intestinal immune homeostasis. Mucosal Immunol. 10, 1518–1528. [PubMed: 28327618]
39. Crowl JT, Heeg M, Ferry A, Milner JJ, Omilusik KD, Toma C, He Z, Chang JT, and Goldrath AW (2022). Tissue-resident memory CD8+ T cells possess unique transcriptional, epigenetic and functional adaptations to different tissue environments. Nat. Immunol. 23, 1121–1131. [PubMed: 35761084]
40. Bai A, Hu H, Yeung M, and Chen J (2007). Krüppel-like factor 2 controls T cell trafficking by activating L-selectin (CD62L) and sphingosine-1-phosphate receptor 1 transcription. J. Immunol. 178, 7632–7639. [PubMed: 17548599]
41. Mackay LK, Wynne-Jones E, Freestone D, Pellicci DG, Mielke LA, Newman DM, Braun A, Masson F, Kallies A, Belz GT, and Carbone FR (2015). T-Box transcription factors combine with the cytokines TGF-β and IL-15 to control tissue-resident memory T cell fate. Immunity 43, 1101–1111. [PubMed: 26682984]
42. Skon CN, Lee JY, Anderson KG, Masopust D, Hogquist KA, and Jameson SC (2013). Transcriptional downregulation of S1pr1 is required for the establishment of resident memory CD8+ T cells. Nat. Immunol. 14, 1285–1293. [PubMed: 24162775]
43. Casey KA, Fraser KA, Schenkel JM, Moran A, Abt MC, Beura LK, Lucas PJ, Artis D, Wherry EJ, Hogquist K, et al. (2012). Antigen-independent differentiation and maintenance of effector-like resident memory T cells in tissues. J. Immunol. 188, 4866–4875. [PubMed: 22504644]
44. Boivin WA, Cooper DM, Hiebert PR, and Granville DJ (2009). Intracellular versus extracellular granzyme B in immunity and disease: challenging the dogma. Lab. Invest. 89, 1195–1220. [PubMed: 19770840]
45. Solovyev VV, Shahmuradov IA, and Salamov AA (2010). Identification of promoter regions and regulatory sites. Methods Mol. Biol. 674, 57–83.
46. Wang S, Sun H, Ma J, Zang C, Wang C, Wang J, Tang Q, Meyer CA, Zhang Y, and Liu XS (2013). Target analysis by integration of transcriptome and ChIP-seq data with BETA. Nat. Protoc. 8, 2502–2515. [PubMed: 24263090]
47. Li S, Bostick JW, Ye J, Qiu J, Zhang B, Urban JF Jr., Avram D, and Zhou L (2018). Aryl hydrocarbon receptor signaling cell intrinsically inhibits intestinal group 2 innate lymphoid cell function. Immunity 49, 915–928.e5. [PubMed: 30446384]
48. Minsavage GD, Park SK, and Gasiewicz TA (2004). The aryl hydrocarbon receptor (AhR) tyrosine 9, a residue that is essential for AhR DNA binding activity, is not a phosphoresidue but augments AhR phosphorylation. J. Biol. Chem. 279, 20582–20593. [PubMed: 14978034]
49. Swanson HI, and Yang JH (1996). Mapping the protein/DNA contact sites of the Ah receptor and Ah receptor nuclear translocator. J. Biol. Chem. 271, 31657–31665. [PubMed: 8940186]
50. Evans BR, Karchner SI, Allan LL, Pollenz RS, Tanguay RL, Jenny MJ, Sherr DH, and Hahn ME (2008). Repression of Aryl Hydrocarbon Receptor (AHR) signaling by AHR repressor: role

of DNA binding and competition for AHR nuclear translocator. Mol. Pharmacol. 73, 387–398. [PubMed: 18000031]

51. Xiong L, Dean JW, Fu Z, Oliff KN, Bostick JW, Ye J, Chen ZE, Mühlbauer M, and Zhou L (2020). Ahr-Foxp3-RORgt axis controls gut homing of CD4+ T cells by regulating GPR15. Sci. Immunol. 5, eaaz7277. [PubMed: 32532834]
52. Gálvez-Cancino F, López E, Menares E, Díaz X, Flores C, Cáceres P, Hidalgo S, Chovar O, Alcántara-Hernández M, Borgna V, et al. (2018). Vaccination-induced skin-resident memory CD8+ T cells mediate strong protection against cutaneous melanoma. Oncoimmunology 7, e1442163. [PubMed: 29900048]
53. Mami-Chouaib F, Blanc C, Corgnac S, Hans S, Malenica I, Granier C, Tihy I, and Tartour E (2018). Resident memory T cells, critical components in tumor immunology. J. Immunother. Cancer 6, 87. [PubMed: 30180905]
54. Murray IA, Patterson AD, and Perdew GH (2014). Aryl hydrocarbon receptor ligands in cancer: friend and foe. Nat. Rev. Cancer 14, 801–814. [PubMed: 25568920]
55. Xue P, Fu J, and Zhou Y (2018). The aryl hydrocarbon receptor and tumor immunity. Front. Immunol. 9, 286. [PubMed: 29487603]
56. Szabo PA, Levitin HM, Miron M, Snyder ME, Senda T, Yuan J, Cheng YL, Bush EC, Dogra P, Thapa P, et al. (2019). Single-cell transcriptomics of human T cells reveals tissue and activation signatures in health and disease. Nat. Commun. 10, 4706. [PubMed: 31624246]
57. Zaid A, Mackay LK, Rahimpour A, Braun A, Veldhoen M, Carbone FR, Manton JH, Heath WR, and Mueller SN (2014). Persistence of skin-resident memory T cells within an epidermal niche. Proc. Natl. Acad. Sci. USA 111, 5307–5312. [PubMed: 24706879]
58. Lawrence BP, Roberts AD, Neumiller JJ, Cundiff JA, and Woodland DL (2006). Aryl hydrocarbon receptor activation impairs the priming but not the recall of influenza virus-specific CD8+ T cells in the lung. J. Immunol. 177, 5819–5828. [PubMed: 17056506]
59. Winans B, Nagari A, Chae M, Post CM, Ko CI, Puga A, Kraus WL, and Lawrence BP (2015). Linking the aryl hydrocarbon receptor with altered DNA methylation patterns and developmentally induced aberrant antiviral CD8+ T cell responses. J. Immunol. 194, 4446–4457. [PubMed: 25810390]
60. Goudot C, Coillard A, Villani AC, Gueguen P, Cros A, Sarkizova S, Tang-Huau TL, Bohec M, Baulande S, Hacohen N, et al. (2017). Aryl hydrocarbon receptor controls monocyte differentiation into dendritic cells versus macrophages. Immunity 47, 582–596.e6. [PubMed: 28930664]
61. Liu Y, Zhou N, Zhou L, Wang J, Zhou Y, Zhang T, Fang Y, Deng J, Gao Y, Liang X, et al. (2021). IL-2 regulates tumor-reactive CD8+ T cell exhaustion by activating the aryl hydrocarbon receptor. Nat. Immunol. 22, 358–369. [PubMed: 33432230]
62. Liu Y, Liang X, Dong W, Fang Y, Lv J, Zhang T, Fiskesund R, Xie J, Liu J, Yin X, et al. (2018). Tumor-repopulating cells induce PD-1 expression in CD8+ T cells by transferring kynurenine and AhR activation. Cancer Cell 33, 480–494.e7. [PubMed: 29533786]
63. Prasad S, Hu S, Sheng WS, Chauhan P, Singh A, and Lokensgard JR (2017). The PD-1: PD-L1 pathway promotes development of brain-resident memory T cells following acute viral encephalitis. J. Neuroinflammation 14, 82. [PubMed: 28407741]
64. Li C, Zhu B, Son YM, Wang Z, Jiang L, Xiang M, Ye Z, Beckermann KE, Wu Y, Jenkins JW, et al. (2019). The transcription factor Bhlhe40 programs mitochondrial regulation of resident CD8+ T cell fitness and functionality. Immunity 51, 491–507.e7. [PubMed: 31533057]
65. Liikanen I, Lauhan C, Quon S, Omilusik K, Phan AT, Bartrolí LB, Ferry A, Goulding J, Chen J, Scott-Browne JP, et al. (2021). Hypoxia-inducible factor activity promotes antitumor effector function and tissue residency by CD8+ T cells. J. Clin. Invest. 131, e143729. [PubMed: 33792560]
66. Boyd A, Almeida JR, Darrah PA, Sauce D, Seder RA, Appay V, Gorochov G, and Larsen M (2015). Pathogen-specific T cell polyfunctionality is a correlate of T cell efficacy and immune protection. PLoS One 10, e0128714. [PubMed: 26046523]
67. De Groot R, Van Loenen MM, Guislain A, Nicolet BP, Freen-Van Heeren JJ, Verhagen OJHM, Van Den Heuvel MM, De Jong J, Burger P, Van Der Schoot CE, et al. (2019). Polyfunctional

tumor-reactive T cells are effectively expanded from non-small cell lung cancers, and correlate with an immune-engaged T cell profile. Oncoimmunology 8, e1648170. [PubMed: 31646094]

68. Egelston CA, Avalos C, Tu TY, Simons DL, Jimenez G, Jung JY, Melstrom L, Margolin K, Yim JH, Kruper L, et al. (2018). Human breast tumor-infiltrating CD8+ T cells retain polyfunctionality despite PD-1 expression. Nat. Commun. 9, 4297. [PubMed: 30327458]
69. Bowcutt R, Malter LB, Chen LA, Wolff MJ, Robertson I, Rifkin DB, Poles M, Cho I, and Loke P (2015). Isolation and cytokine analysis of lamina propria lymphocytes from mucosal biopsies of the human colon. J. Immunol. Methods 421, 27–35. [PubMed: 25769417]
70. Fernandez-Salguero P, Pineau T, Hilbert DM, McPhail T, Lee SS, Kimura S, Nebert DW, Rudikoff S, Ward JM, and Gonzalez FJ (1995). Immune system impairment and hepatic fibrosis in mice lacking the dioxin-binding Ah receptor. Science 268, 722–726. [PubMed: 7732381]
71. Qiu J, Heller JJ, Guo X, Chen Z.m.E., Fish K, Fu YX, and Zhou L (2012). The aryl hydrocarbon receptor regulates gut immunity through modulation of innate lymphoid cells. Immunity 36, 92–104. [PubMed: 22177117]
72. Fu Z, Dean JW, Xiong L, Dougherty MW, Oliff KN, Chen ZME, Jobin C, Garrett TJ, and Zhou L (2021). Mitochondrial transcription factor A in RORgt^{+} lymphocytes regulate small intestine homeostasis and metabolism. Nat. Commun. 12, 4462. [PubMed: 34294718]
73. Dobin A, Davis CA, Schlesinger F, Drenkow J, Zaleski C, Jha S, Batut P, Chaisson M, and Gingeras TR (2013). STAR: ultrafast universal RNA-seq aligner. Bioinformatics 29, 15–21. [PubMed: 23104886]
74. Li B, and Dewey CN (2011). RSEM: accurate transcript quantification from RNA-Seq data with or without a reference genome. BMC Bioinformatics 12, 323. [PubMed: 21816040]
75. Love MI, Huber W, and Anders S (2014). Moderated estimation of fold change and dispersion for RNA-seq data with DESeq2. Genome Biol. 15, 550. [PubMed: 25516281]
76. Subramanian A, Tamayo P, Mootha VK, Mukherjee S, Ebert BL, Gillette MA, Paulovich A, Pomeroy SL, Golub TR, Lander ES, and Mesirov JP (2005). Gene set enrichment analysis: a knowledge-based approach for interpreting genome-wide expression profiles. Proc. Natl. Acad. Sci. USA 102, 15545–15550. [PubMed: 16199517]
77. Mootha VK, Lindgren CM, Eriksson KF, Subramanian A, Sihag S, Lehar J, Puigserver P, Carlsson E, Ridderstråle M, Laurila E, et al. (2003). PGC-1α-responsive genes involved in oxidative phosphorylation are coordinately downregulated in human diabetes. Nat. Genet. 34, 267–273. [PubMed: 12808457]
78. R Core Team (R Foundation for Statistical Computing, Vienna, Austria. 2022). R: A Language and Environment for Statistical Computing.
79. Murdoch D, and Adle D rgl: 3D Visualization Using OpenGL. R package. 2021.
80. Kolde R (R package. 2019). Pheatmap: Pretty Heatmaps.
81. Langmead B, and Salzberg SL (2012). Fast gapped-read alignment with Bowtie 2. Nat. Methods 9, 357–359. [PubMed: 22388286]
82. Li H, Handsaker B, Wysoker A, Fennell T, Ruan J, Homer N, Marth G, Abecasis G, and Durbin R; 1000 Genome Project Data Processing Subgroup (2009). The sequence alignment/map format and SAMtools. Bioinformatics 25, 2078–2079. [PubMed: 19505943]
83. Quinlan AR, and Hall IM (2010). BEDTools: a flexible suite of utilities for comparing genomic features. Bioinformatics 26, 841–842. [PubMed: 20110278]
84. Heinz S, Benner C, Spann N, Bertolino E, Lin YC, Laslo P, Cheng JX, Murre C, Singh H, and Glass CK (2010). Simple combinations of lineage-determining transcription factors prime cis-regulatory elements required for macrophage and B cell identities. Mol. Cell 38, 576–589. [PubMed: 20513432]
85. Butler A, Hoffman P, Smibert P, Papalexi E, and Satija R (2018). Integrating single-cell transcriptomic data across different conditions, technologies, and species. Nat. Biotechnol. 36, 411–420. [PubMed: 29608179]
86. Trapnell C, Cacchiarelli D, Grimsby J, Pokharel P, Li S, Morse M, Lennon NJ, Livak KJ, Mikkelsen TS, and Rinn JL (2014). The dynamics and regulators of cell fate decisions are revealed by pseudotemporal ordering of single cells. Nat. Biotechnol. 32, 381–386. [PubMed: 24658644]

Highlights

- Ahr acts as a promoter of resident memory $CD8^+$ T cell differentiation and function
- Ahr suppresses the circulating but promotes the resident memory core gene program
- Ahr enhances polyfunctional $CD8^+$ T cells, which drive anti-tumor immunity
- In human, AHR promotes *in vitro* T_{RM} differentiation and granzyme B production

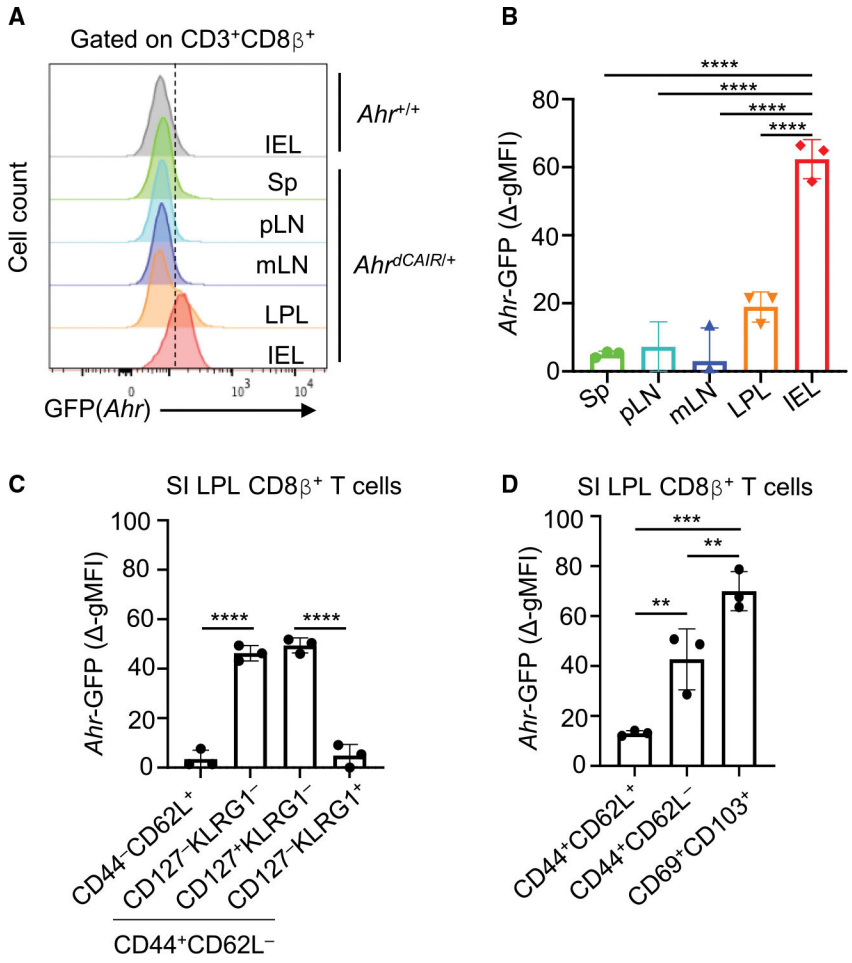

Figure 1. Ahr is expressed by intestinal resident CD8αβ T cells

(A and B) Flow cytometry analysis of *Ahr* expression (GFP) in CD8$^+$ T cells of *Ahr*$^{+/+}$ and *Ahr*$^{dCAIR/+}$ mice was performed. Histogram plot of GFP(*Ahr*) in CD8$^+$ T cells isolated from spleen (Sp), peripheral lymph node (pLN), mesenteric lymph node (mLN), small intestine lamina propria (LPL), or intraepithelial lymphocytes (IEL) (A). Quantification of ΔgMFI in *Ahr*$^{dCAIR/+}$ compared with GFP-negative *Ahr*$^{+/+}$ mice (B).

(C and D) Flow cytometry quantification of ΔgMFI of *Ahr*-GFP in different CD8$^+$ T cell populations isolated from LPL including CD44$^-$CD62L$^+$ (T_{naive}), CD127$^-$KLRG1$^-$ (T_{EE}), CD127$^-$KLRG1$^+$ (T_{SLE}), CD127$^+$KLRG1$^-$ (T_{MPE}) (C), and CD44$^+$CD62L$^+$ (T_{CM}), CD44$^+$CD62L$^-$ (T_{EM}), and CD69$^+$CD103$^+$(T_{RM}) (D). Data are shown as mean ± SEM (n = 3 mice per group). Data are representative of two independent experiments. See also Figure S1.

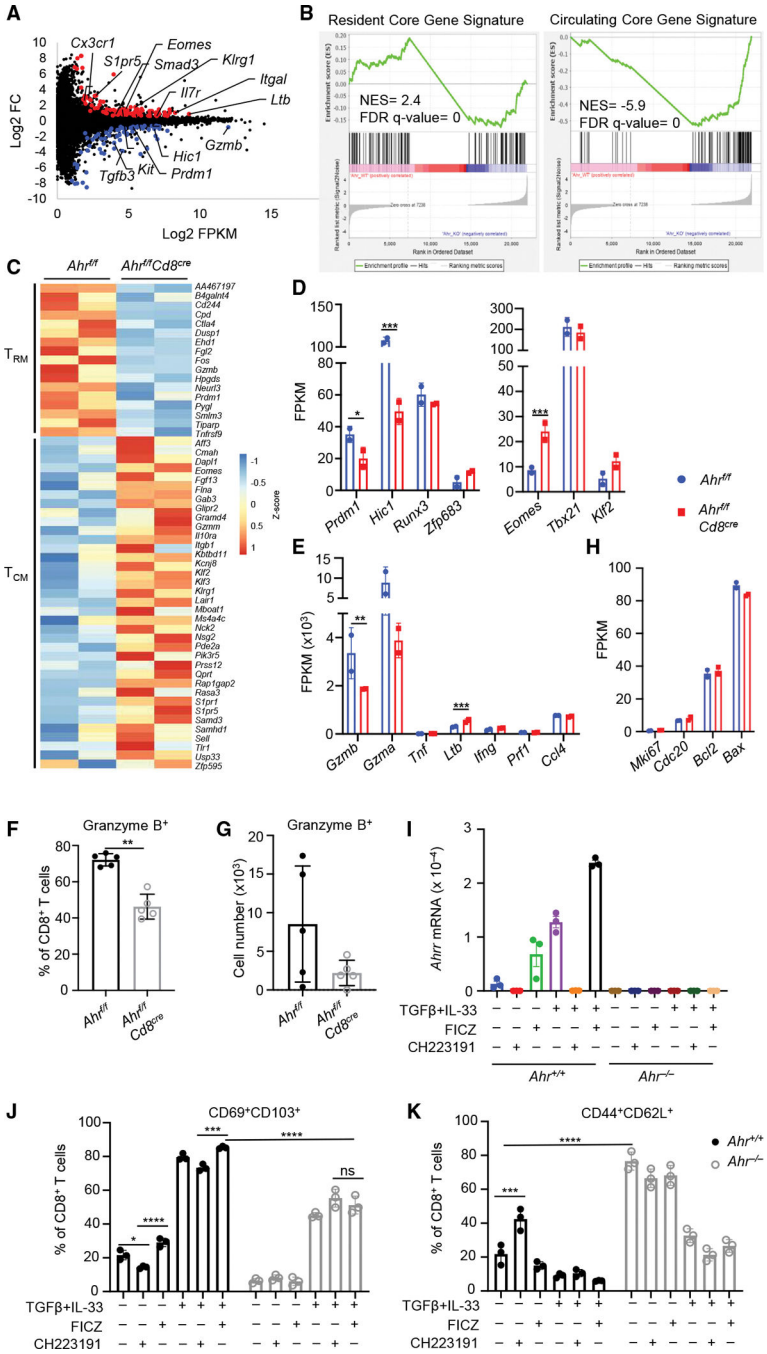

Figure 2. Ahr suppresses T_{CM} while promoting T_{RM} gene signature in intestinal CD8$^+$ T cells

(A–E and H) RNA-seq analysis of IEL resident CD8$^+$ T cells isolated from *Ahr*$^{f/f}$ and *Ahr*$^{f/f}$*Cd8*^{cre} mice and statistics (q values shown) were calculated via DESeq2 differential expression analysis, and FPKM values were quantified using RSEM. MA plot highlighting genes upregulated (red) and downregulated (blue) in *Ahr*$^{f/f}$*Cd8*^{cre} compared with *Ahr*$^{f/f}$ (A). Gene set enrichment analysis of resident and circulating core gene signatures (B). Heatmap depicting (fold change >1.5) genes enriched in respective signatures (C). FPKM expression

values for transcriptional regulators (D) and secreted factors associated with cell function (E).

(F and G) Flow cytometry quantification of granzyme B protein levels of IEL resident $CD8^+$ T cells isolated from $Ahr^{f/f}$ and $Ahr^{f/f}Cd8^{cre}$ mice. The percentages (F) and total cell number (n = 5 mice per group) (G) are shown. Data are representative of two independent experiments.

(H) FPKM expression values for proliferation, cell cycle, and apoptosis genes.

(I–K) Naive $CD8^+$ T cells were isolated from $Ahr^{+/+}$ and $Ahr^{-/-}$ mice and then subjected to *in vitro* T_{RM}-like differentiation culture conditions. RNA was isolated for qRT-PCR expression analysis of *Ahrr* (I). Flow cytometry quantification of $CD69^+CD103^+$ *in vitro* T_{RM}-like cells (J) and $CD44^+CD62L^+$ *in vitro* T_{CM}-like population frequency (K). Data are shown as mean ± SEM (n = 3 mice per group). Data are representative of three independent experiments. See also Figures S1, S2, and S3.

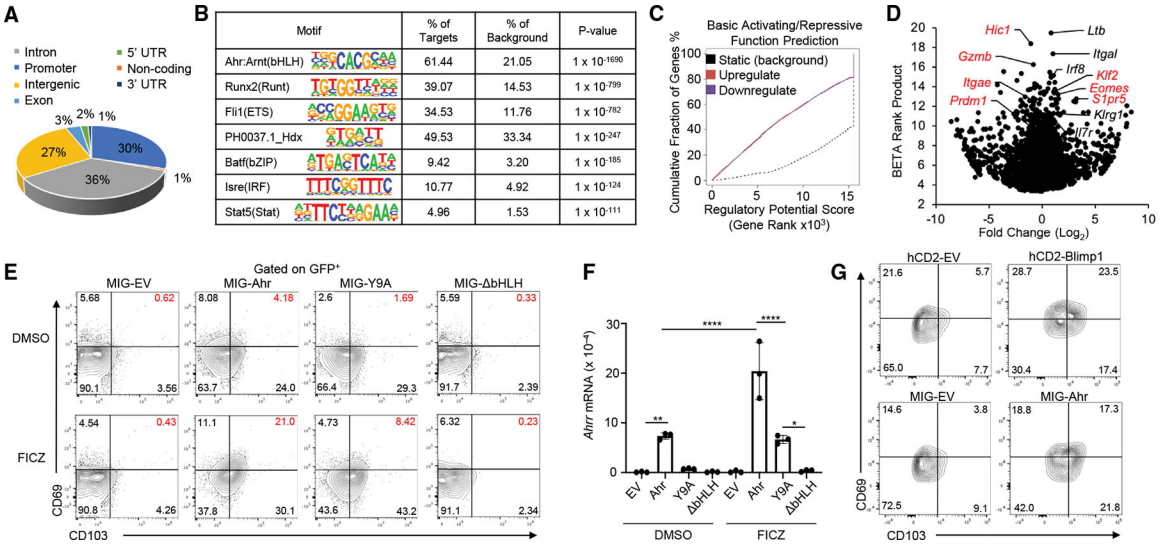

Figure 3. Ahr directly binds DNA to regulate key T_{RM} genes

(A and B) ChIP-seq of Ahr was performed using *in vitro* T_{RM}-like $CD8^+$ T cells. Analysis of Ahr binding was performed, and pie chart of peak annotation (A) as well as top seven enriched transcription factor motifs (B) are shown.

(C and D) Binding and Expression Target Analysis (BETA) was performed to integrate RNA-seq and ChIP-seq data. Visualization of transcription factor activating/repressive function prediction (C) and rank product volcano plot depicting top direct target candidates (D).

(E and F) *Ahr*$^{-/-}$ *in vitro* T_{RM}-like $CD8^+$ T cells transduced with retroviral constructs encoding MIG-EV (empty vector), MIG-Ahr, MIG-Y9A, or MIG-DbHLH. The cells were treated with DMSO or FICZ on day 3. On day 5, CD69 and CD103 expression was analyzed by flow cytometry (E), and RNA was isolated for qRT-PCR expression analysis of Ahr direct target gene *Ahrr* (F). Data are shown as mean ± SEM (n = 3 technical replicates per group). Data are representative of two independent experiments.

(G) Flow cytometry analysis of CD69 and CD103 expression in *Ahr*$^{-/-}$ *in vitro* T_{RM}-like $CD8^+$ T cells transduced with retroviral constructs encoding MIG-EV, MIG-Ahr, hCD2-EV, or hCD2-Blimp1. Data are representative of two independent experiments. See also Figure S5.

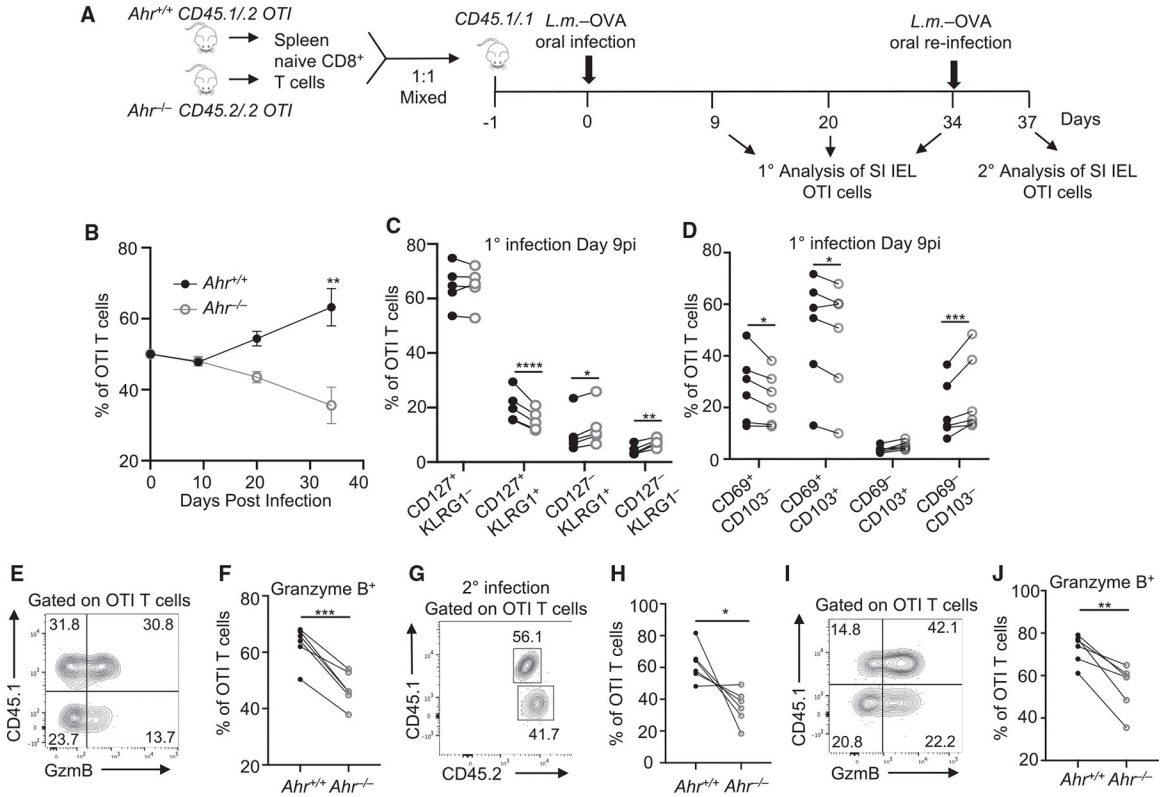

Figure 4. Ahr is a cell-intrinsic promoter of intestinal CD8$^+$ T_{RM} during infection

(A–F) Analysis of antigen-specific (OTI) CD8$^+$ T cell response in the IEL during oral *L.m.*-OVA infection was performed as depicted in the schematic (A). Flow cytometry quantification of the percentage of *Ahr*$^{+/+}$ vs. *Ahr*$^{-/-}$ OTI cells on day 9, 20, and 34 post infection (B). Flow cytometry quantification of memory precursor populations based on expression of CD127 and KLRG1 (C) as well as CD69 and CD103 (D) in *Ahr*$^{+/+}$ vs. *Ahr*$^{-/-}$ OTI cells present in the IEL on day 9 post infection. Flow cytometry analysis of CD45.1 and GzmB gated on OTI cells depicting *CD45.1*$^+$ *Ahr*$^{+/+}$(CD45.1/.2) and *CD45.1*$^-$ *Ahr*$^{-/-}$(CD45.2/.2) OTI cells production of granzyme B on day 34 post infection (E). Quantification of granzyme B$^+$ OTI T cells in the mice of indicated genotypes (F). (G–J) *L.m.*-OVA re-infection was performed and *Ahr*$^{+/+}$ vs. *Ahr*$^{-/-}$ OTI IEL resident CD8$^+$ T cells analyzed on day 3 post re-infection. Flow cytometry analysis of CD45.1 and CD45.2 depicting percentage of *Ahr*$^{+/+}$(CD45.1/.2) and *Ahr*$^{-/-}$(CD45.2/.2) OTI IEL resident CD8$^+$ T cells as well as (G) quantification of percentage are shown (H). Flow cytometry analysis (I) and quantification (J) of granzyme B production in analyzed cells. Data are compiled from two independent experiments and shown as mean ± SEM (n = 3–6 replicates per group). See also Figure S6.

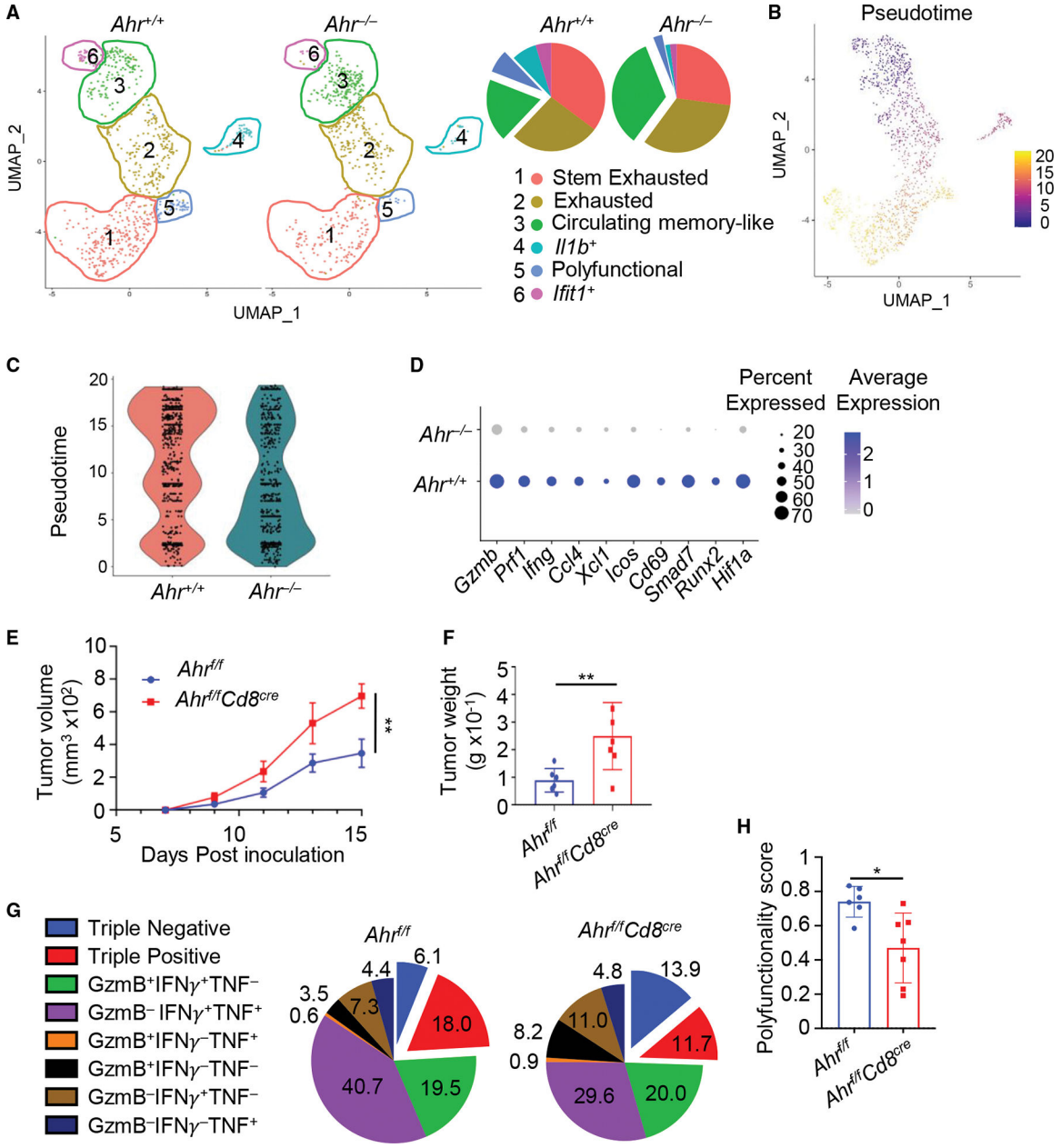

Figure 5. Single-cell RNA-seq identifies polyfunctional CD8$^+$ T cell population dependent on Ahr

(A–D) scRNA-seq analysis of *Ahr*$^{+/+}$ (n = 2) vs. *Ahr*$^{-/-}$ (n = 2) TIL CD8$^+$ T cells was performed. UMAP dimensionality reduction and cluster visualization (left) as well as pie chart frequency depiction (right) color-coded to represent cluster ID (A). Pseudotime visualization (B) and quantification (C). Differential gene expression depicted via color intensity as average expression and circle size as percent expressed in CD8$^+$ T cells (D). (E–H) *Ahr*$^{f/f}$ and *Ahr*$^{f/f}$*Cd8*^{cre} mice were inoculated subcutaneously with B16F10 mouse melanoma and tumor size monitored (E). At endpoint, tumor weight was quantified (F), and TILs were isolated for flow cytometry analysis. Pie chart visualization depicting polyfunctionality of TIL CD8$^+$ T cells in mice with indicated genotypes (G). Polyfunctionality score quantification (triple-positive plus double-positive minus triple-

negative divided by total cells) of TIL CD8$^+$ T cells isolated from *Ahr*$^{f/f}$ and *Ahr*$^{f/f}$*Cd8*^{cre} tumor-bearing mice (H). Data are compiled from two independent experiments and are shown as mean ± SEM (n = 6 to 7 replicates per group). See also Figure S7.

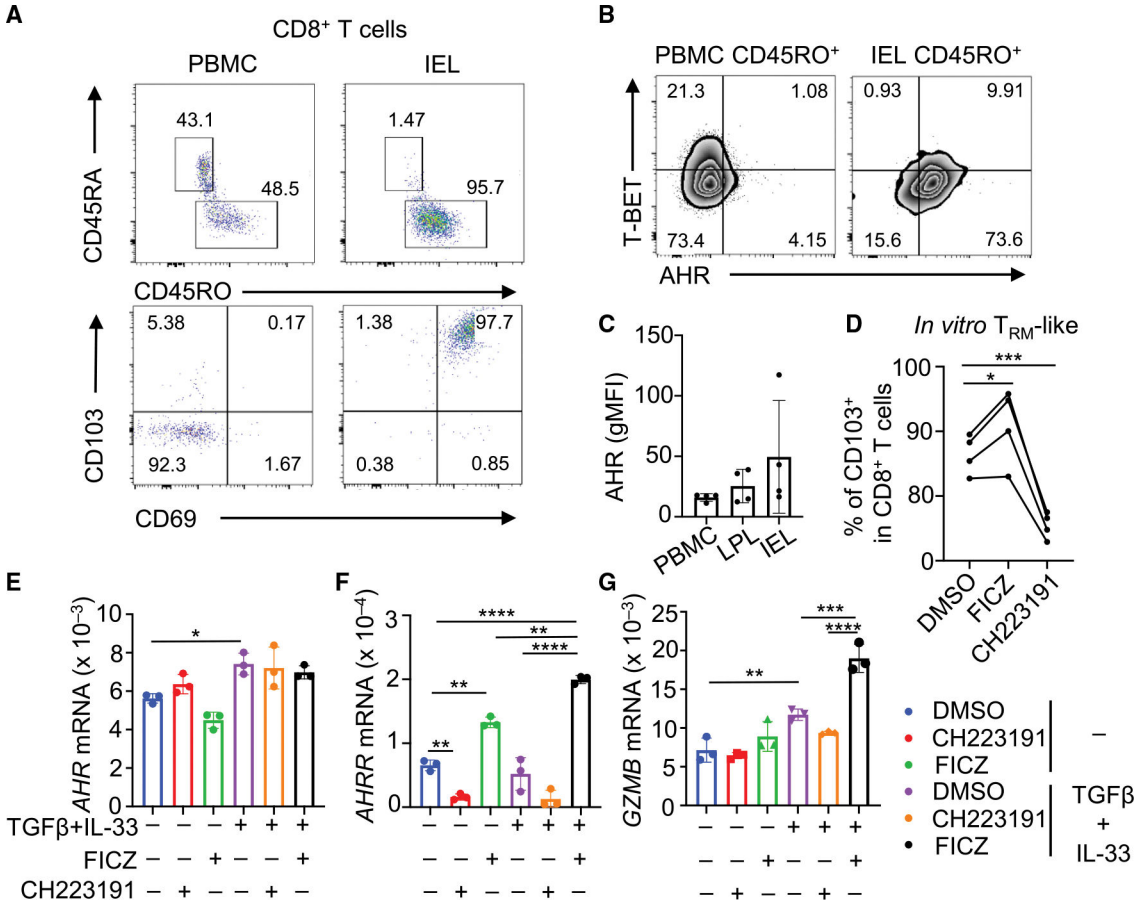

Figure 6. AHR signaling promotes T_{RM} differentiation and function in human CD8 T cells

(A–C) Human peripheral blood (PBMC) vs. IEL CD8$^+$ T cells were analyzed via flow cytometry. Staining of CD45RA and CD45RO (top), CD103 and CD69 (bottom) (A), as well as T-BET and AHR (B) in tissue fractions as indicated in the figure. Quantification of AHR protein levels (gMFI) in human PBMC, LPL, and IEL CD8$^+$ T cells (C). Data are compiled from three independent experiments and shown as mean ± SEM (n = 4 replicates per group).

(D–G) Human naive CD8$^+$ T cells were isolated from PBMCs and then subjected to *in vitro* T_{RM}-like differentiation culture conditions. The cells were given differentiation cytokines and treated with DMSO (control), FICZ, or CH223191 on day 2. The assay was collected on day 4, and flow cytometry quantification of CD103 expression was performed (D). Data are compiled from three independent experiments and are shown as mean ± SEM (n = 4 replicates per group). RNA was isolated for qRT-PCR expression analysis of *AHR* (E), AHR direct target gene *AHRR* (F), and *GZMB* (G). Data are shown as mean ± SEM (n = 3 technical replicates per group). Data are representative of three independent experiments.

KEY RESOURCES TABLE

REAGENT or RESOURCE	SOURCE	IDENTIFIER
Antibodies		
Anti-mouse CD45.2 – FITC (clone 104)	TONBO biosciences	Cat# 35-0454-U500; RRID: AB_2621692
Anti-mouse CD45.1 – APC/Cyanine7 (clone A20)	BioLegend	Cat# 110716; RRID: AB_313505
Anti-mouse TCRβ – Brilliant Violet 650 (clone H57-597)	BioLegend	Cat# 109251; RRID: AB_2810348
Anti-mouse TCRβ – eFluor 450 (clone H57-597)	Invitrogen	Cat# 48-5961-82; RRID: AB_11039532
Anti-mouse CD3e – FITC (clone 145-2C11)	TONBO biosciences	Cat# 35-0031-U500; RRID: AB_2621659
Anti-mouse CD3 – APC-eFluor 780 (clone 17A2)	Invitrogen	Cat# 47-0032-82; RRID: AB_1272217
Anti-mouse CD8b – FITC (clone YTS156.7.7)	BioLegend	Cat# 126606; RRID: AB_961295
Anti-mouse CD8b – Brilliant Violet 711 (clone YTS156.7.7)	BioLegend	Cat# 126633; RRID: AB_2800622
Anti-mouse CD8a – APC/Cyanine7 (clone 53-6.7)	BioLegend	Cat# 100714; RRID: AB_312753
Anti-mouse CD8a – Brilliant Violet 605 (clone 53–6.7)	BioLegend	Cat# 100744; RRID: AB_2562609
Anti-mouse/human CD44 – Brilliant Violet 421 (clone IM7)	BioLegend	Cat# 103040; RRID: AB_2616903
Anti-mouse CD62L – PE-Cyanine7 (clone MEL-14)	Invitrogen	Cat# 25-0621-82; RRID: AB_469633
Anti-mouse CD127 – PE/Dazzle 594 (clone A7R34)	BioLegend	Cat# 135032; RRID: AB_2564217
Anti-mouse KLRG1 – PerCP-eFluor 710 (clone 2F1)	Invitrogen	Cat# 46-5893-82; RRID: AB_10670282
Anti-mouse CD69 – Brilliant Violet 711 (clone H1.2F3)	BioLegend	Cat# 104537; RRID: AB_2566120
Anti-mouse CD69 – PE (clone H1.2F3)	Invitrogen	Cat# 12-0691-82; RRID: AB_465732
Anti-mouse CD103 – Brilliant Violet 785 (clone 2E7)	BioLegend	Cat# 121439; RRID: AB_2800588
Anti-mouse CD103 – APC (clone 2E7)	Invitrogen	Cat# 17-1031-82; RRID: AB_1106992
Anti-human/mouse Granzyme B – Pacific Blue (clone GB11)	BioLegend	Cat# 515408; RRID: AB_2562196
Anti-human/mouse Granzyme B – Alexa Fluor 700 (clone QA16A02)	BioLegend	Cat# 372222; RRID: AB_2728389
Anti-mouse IFN gamma – PerCP-Cyanine5.5 (clone XMG1.2)	Invitrogen	Cat# 45-7311-82; RRID: AB_1107020
Anti-mouse TNF – PE-Cyanine7 (clone MP6-XT22)	Invitrogen	Cat# 25-7321-82; RRID: AB_11042728
Anti-mouse Ki-67 – Brilliant Violet 605 (clone 16A8)	BioLegend	Cat# 652413; RRID: AB_2562664
Anti-mouse Ki-67 – Alexa Fluor 647 (clone B56)	BD	Cat# 558615; RRID: AB_647130
Anti-mouse Eomes – PE-Cyanine7 (clone Dan11mag)	Invitrogen	Cat# 25-4875-82; RRID: AB_2573454
Anti-mouse Ahr – eFluor 660 (clone 4MEJJ)	Invitrogen	Cat# 50-5925-82; RRID: AB_2574255
Anti-mouse Ahr – Alexa Fluor 488 (clone 4MEJJ)	Invitrogen	Cat# 53-5925-82; RRID: AB_2574425
Anti-mouse Blimp1 – APC (clone 5E7)	BioLegend	Cat# 150007; RRID: AB_2728186
Anti-Annexin V – APC	eBioscience	Cat# 17-8007-74
Anti-Annexin V – PE/Dazzle 594	BioLegend	Cat# 640955
Anti-human CD3 – FITC (clone SK7)	TONBO biosciences	Cat# 35-0036-T025; RRID: AB_2621661
Anti-human CD8 – APC-Cyanine7 (clone SK1)	TONBO biosciences	Cat# 25-0087-T025; RRID: AB_2848136
Anti-human CD45RA – PerCP-Cyanine5.5 (clone HI100)	TONBO biosciences	Cat# 65-0458-T100; RRID: AB_2621896
Anti-human CD45RO – Brilliant Violet 605 (clone UCHL1)	BioLegend	Cat# 304237; RRID: AB_2562143
Anti-human CD197 – Brilliant Violet 711 (clone G043H7)	BioLegend	Cat# 353227; RRID: AB_11219587
Anti-human CD127 – PE/Dazzle 594 (clone A019D5)	BioLegend	Cat# 351335; RRID: AB_2563636
Anti-human CD69 – Brilliant Violet 785 (clone FN50)	BioLegend	Cat# 310931; RRID: AB_2561370
Anti-human CD103 – APC (clone Ber-ACT8)	BioLegend	Cat# 350215; RRID: AB_2563906

REAGENT or RESOURCE	SOURCE	IDENTIFIER
Anti-human AhR – PE (clone T49-550)	BD	Cat# 565711; RRID: AB_2739336
Anti-human T-bet – Brilliant Violet 421 (clone 4B10)	BioLegend	Cat# 644815; RRID: AB_10896427
Anti-human CD2 – eFluor 450 (clone RPA-2.10)	Invitrogen	Cat# 48-0029-42; RRID: AB_2574006
anti-mouse Ahr (polyclonal)	Enzo Life Science	Cat# BML-SA210–0100; RRID: AB_10540536
Bacterial and virus strains		
L.m.-OVA InlAM	Sheridan et al., 2014[3]	N/A
Biological samples		
Human PBMC isolated from buffy coats	Life South Community Blood Centers	https://www.lifesouth.org/
Human colon tissue biopsies	UFHealth Inflammatory Bowel and Celiac Disease Program	https://ufhealth.org/comprehensive-inflammatory-bowel-diseases-program/overview
Chemicals, peptides, and recombinant proteins		
Recombinant Murine IL-2	PeproTech	Cat# 212-12
Recombinant Murine IL-33	PeproTech	Cat# 210-33
Recombinant Human TGF-β	PeproTech	Cat# 100-21
Recombinant Human IL-2	PeproTech	Cat# 200-02
Recombinant Human IL-33	PeproTech	Cat# 200-33
6-formylindolo(3.2b) carbazole (FICZ)	Sigma	Cat# SML 1489-5MG
CH223191	Sigma	C8124-5MG
Critical commercial assays		
TRIzol Reagent	Invitrogen	Cat# 15596018
iQ SYBR Green Supermix	Biorad	Cat# 1708887
Nextera DNA Library Preparation Kit	Illumina	Cat# FC-121-1030
NEBNext High-Fidelity 2X PCR Master Mix	NEB	Cat# M0541
SMART-Seq HT Kit	Takara	Cat# 634456
iDeal ChIP-Seq	Diagenode	Cat# C01010055
GoScript Reverse Transcriptase	Promega	Cat# A5003
Zombie Aqua Fixable Viability Kit	BioLegend	Cat# 423102
Live and Dead Violet Viability Kit	Invitrogen	Cat# L34955
Foxp3/Transcription Factor Staining Buffer Set	eBioscience	Cat# 00-5523-00
Dynabeads Mouse T-Activator CD3/CD28	Thermo Fisher	Cat# 11452D
Dynabeads Human T-Activator CD3/CD28	Thermo Fisher	Cat# 11131D
Deposited data		
RNA-Seq, ChIP-Seq, scRNA-Seq	This paper	GEO: GSE220944
Experimental models: Cell lines		

REAGENT or RESOURCE	SOURCE	IDENTIFIER
B16F10	ATCC	CRL-6475
MC38	Kerafast	ENH204-FP
Experimental models: Organisms/strains		
Mouse: CD45.1/1	The Jackson Laboratory	Cat# 002014
Mouse: *Ahr*$^{-/-}$	Fernandez-Salguero et al.	N/A
Mouse: AhrdCAIR	Ye et al., 2017[36]	N/A
Mouse: *EI8Cre*	The Jackson Laboratory	Cat# 008766
Mouse: Ahrf/f	The Jackson Laboratory	Cat# 035734
Mouse: OTI TCR transgenic	The Jackson Laboratory	Cat# 003831
Oligonucleotides		
See Table S1 for list of quantitative RT-PCR primers	This paper	N/A
Recombinant DNA		
Plasmid: MIG-EV	Xiong et al., 2020[51]	N/A
Plasmid: MIG-Ahr	Xiong et al., 2020[51]	N/A
Plasmid: MIG-Y9A	Xiong et al., 2020[51]	N/A
Plasmid: MIG-ΔbHLH	Xiong et al., 2020[51]	N/A
Plasmid: hCD2-EV	Laboratory of Dr. Weishan Huang	N/A
Plasmid: hCD2-Blimp1	Laboratory of Dr. Weishan Huang	N/A
Software and algorithms		
FlowJo version 10.4.2	FlowJo	https://www.flowjo.com
Prism 8	GraphPad Software	https://www.graphpad.com/scientific-software/prism/